GLD1724

LBL-11836
UC-66a

Lawrence Berkeley Laboratory
UNIVERSITY OF CALIFORNIA

EARTH SCIENCES DIVISION

CONSTANT PRESSURE CHARGING OF A LIQUID DOMINATED GEOTHERMAL RESERVOIR

K.P. Goyal and T.N. Narasimhan

March 1982

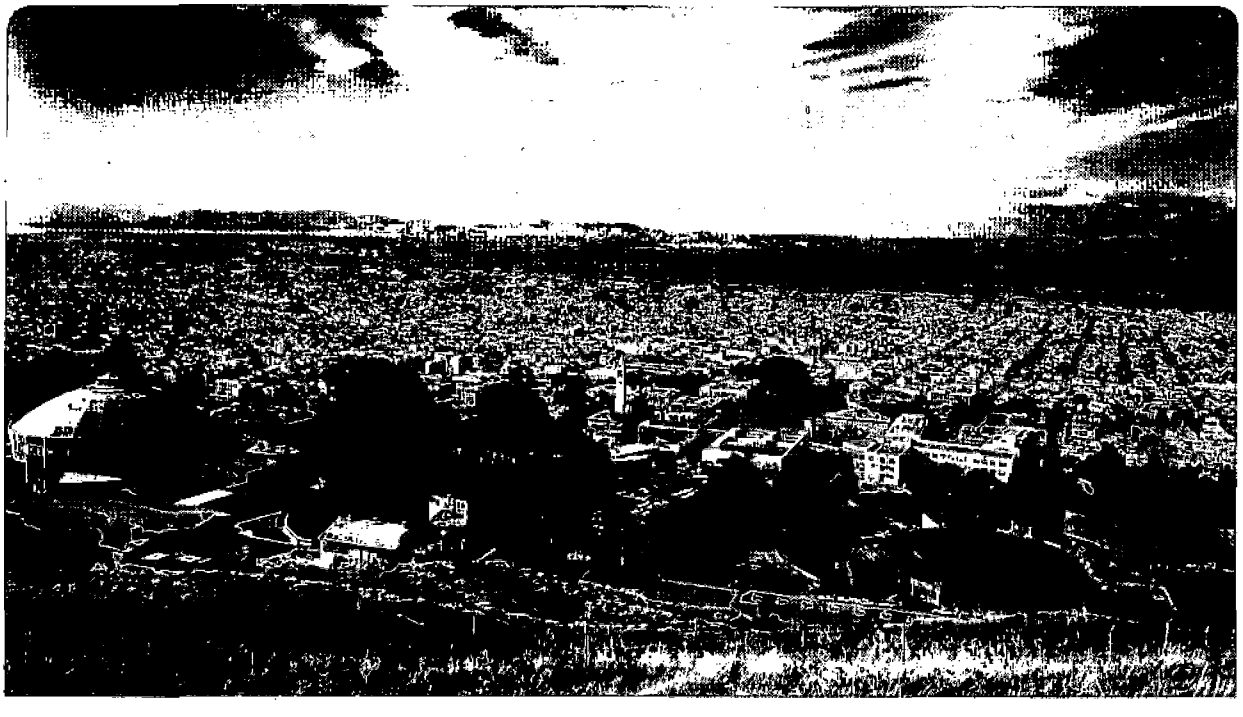

Prepared for the U.S. Department of Energy under Contract DE-AC03-76SF00098

Printed in the United States of America
Available from
National Technical Information Service
U.S. Department of Commerce
5285 Port Royal Road
Springfield, VA 22161
Price Code: A04

LBL-11836

CONSTANT PRESSURE CHARGING OF A LIQUID DOMINATED GEOTHERMAL RESERVOIR

K. P. Goyal and T. N. Narasimhan

Lawrence Berkeley Laboratory
University of California
Berkeley, California 94720

This work was supported by the Assistant Secretary for Conservation and Renewable Energy, Office of Renewable Technology, Division of Geothermal and Hydropower Technologies, of the U. S. Department of Energy under Contract No. DE-AC03-76SF00098.

CONSTANT PRESSURE CHARGING OF A LIQUID DOMINATED GEOTHERMAL RESERVOIR

K. P. Goyal and T. N. Narasimhan

Earth Sciences Division, Lawrence Berkeley Laboratory
University of California, Berkeley, California 94720

ABSTRACT

A two-dimensional mathematical model of a fault controlled geothermal reservoir has been developed. Heated water rising in a fault, is assumed to charge a reservoir which is overlain by a thin impermeable, thermally conducting cap rock. The mass flow rate or the pressure associated with the charging process at the fault inlet is unknown and can only be estimated. Thus, in this paper, the pressure in the fault at the bottom of the reservoir is assumed to be prescribed. Quasi-analytic solutions for the distributions of velocity, pressure, and temperature are obtained in the fault-reservoir system for high Rayleigh number flow. In this approximation, the upwelling fluid does not cool off appreciably until it reaches the cold upper boundary of the reservoir and encounters conductive heat loss. The thermal boundary layer, which is thin at the top of the fault, grows outward laterally and occupies the full thickness of the aquifer in the far-field. An interesting consequence of this work relates to the interpretation of the temperature profiles in the aquifer. This study shows that a near isothermal temperature profile, in the aquifer-region close to the fault, can result due to significant horizontal velocities as opposed to the conventional intuitive interpretation of strong vertical mixing due to convection. An interpretation of data from over a dozen wells from East Mesa geothermal field

in California seems to qualitatively support the model suggested in the present work. It appears that model will be of value in the preliminary analysis of geothermal reservoirs elsewhere using initial exploratory data such as surface heat flow, static temperature profiles and bottomhole shut-in pressures.

NOMENCLATURE

A	Constant, defined in Equation (29)
b_1	Constant, defined in Equation (17b)
C_1	Constant, defined in Equation (17a)
C_p'	specific heat of the liquid at constant pressure, $m^2/sec\text{-}K$
d	An O (1) number [Equation (8)]
g'	acceleration due to gravity, m/sec^2
H'	Half width of the reservoir in y-direction, m
K'	fault permeability and horizontal permeability in the aquifer, m^2
L'	depth of the reservoir, m
M'	mass flow rate per unit length in the direction perpendicular to the plane of paper, kg/m-sec
p'	fluid pressure in the aquifer, Pascals
P'	fluid pressure in the fault, Pascals
P_b'	specified fluid pressure in the fault at $z' = -L'$, Pascals
P_H'	cold hydrostatic fluid pressure with respect to density ρ_o', Pascals
ρ_o'	Reference convection pressure [Equation (2)]
q_o'	Reference convection velocity [Equation (2)]
R	Rayleigh number [Equation (2)]
T'	fault temperature, K
T_{max}'	maximum temperature at the hot bottom boundary of the reservoir, K
T_o'	ambient temperature, K

v'	horizontal Darcy mass flux in the aquifer per unit area, kg/m^2-sec
V'	horizontal Darcy mass flux in the fault per unit area, kg/m^2-sec
W'	vertical Darcy mass flux in the fault per unit area, kg/m^2-sec
y'	horizontal distance in y-direction, m
z'	vertical distance in z-direction, m
y_e'	semifault width, m
α_e'	coefficient of thermal expansion of the liquid, K^{-1}
γ	An O (1) number [Equation (4b)]
$\Delta T'$	maximum temperature difference across the aquifer = $T_{max}' - T_o'$, K
θ'	aquifer temperature, K
λ_m'	thermal conductivity of the porous medium, Kg-m/sec^3-K
ν'	kinematic viscosity, m^2/sec
ρ'	density of the liquid at the temperature T', kg/m^3
ρ_o'	density of the liquid at the ambient temperature T_o', kg/m^3
	overheat ratio [Equation (1)]

INTRODUCTION

The analysis of available geophysical data from various geothermal systems has made it possible to develop conceptual reservoir models which contain elements of physical plausibility. Such availability has helped to evolve extremely idealized mathematical models for heat and mass transfer in unexploited liquid dominated geothermal systems in a form which is at least physically viable. The hypothetical idealized models, developed by extensions of classical hydrodynamic stability theory in porous media (see review articles by Combarnous and Bories [1], Cheng [2], Garg and Kassoy [3]) lack both the significant internal structure and boundary conditions relevant to real geothermal systems and thus preclude the comparison of theoretical prediction with field measurements. For example, the convective configuration associated with an incompletely defined system (infinite slab configuration) or simplified thermal boundary condition (uniform temperature on a horizontal boundary) may not resemble those obtained in real systems where geological structure (the combination of fracture zones, faults and aquifers), boundary irregularity and localized intrusive bodies may have a significant effect on the flow dynamics.

Hypothetical, but more plausible models, containing the elements of configurational, structural and thermal reality have developed into a variety of ways since the pipe models of Einarsson [4], Wooding [5], Elder [6] and Donaldson [7,8]. Such models have been surveyed by Goyal and Kassoy [9]. Einarsson's pipe model concept arises from the hydrodynamic imbalance that exists between the heated, low density

water in the active part of a geothermal reservoir and the colder, denser water in the peripheral region.

Attempts have been made in the literature to develop models of exploited and unexploited geothermal systems on the basis of known field data. Such models include Wooding's [5] cross-sectional model of upflow in the Wairakei system; the two-dimensional areal reservoir model for Wairakei by Mercer et al. [10] and Mercer and Faust [11]; Sorey's [12] large-scale vertical model of the Long Valley Caldera, The Salton Sea reservoir areal model developed by Riney et al. [13], three dimensional model of the Cerro Prieto field by Lippmann and Goyal [14], two dimensional vertical model of the Wairakei system by Pritchett et al. [15], a vertical profile analysis of the East Mesa system by Goyal [16] and Goyal and Kassoy [17] and a fault controlled two dimensional model of Susanville hydrothermal system by Benson et al. [27].

In this paper we present a two-dimensional generic model similar to that of Goyal and Kassoy [9], for a liquid dominated geothermal reservoir charged by heated water through a vertical fault zone. The reservoir is assumed to underlie a thin, thermally conducting caprock. Earlier, Goyal and Kassoy [9] considered a constant flux boundary condition at the bottom of the fault. In the present study, however, we assume a boundary condition such that the pressure in the fault at the bottom of the reservoir is prescribed. Additionally, the analysis can also be used to compute the velocity field in response to changes in viscosity or permeability under a prescribed pressure gradient. This boundary condition is practically realistic since it is far easier to measure reservoir fluid pressures than fluid fluxes or

velocities. The governing equations pertain to heat and mass transfer in saturated permeable media. The solution technique used involves a combination of perturbation methods, boundary layer theory and numerical methods. Results are presented for distribution of pressures, velocities, temperatures and temperature gradients in the system. The application of the theory to a typical geothermal system is discussed in the last section.

DEVELOPMENT OF CONCEPTUAL MODEL

Studies of liquid-dominated geothermal systems such as those at Wairakei (Grindley [18]), Broadlands (Grindley [19]), Long Valley (Rinehart and Ross [20]), Imperial Valley (Elders et al. [21]), Cerro Prieto (Puente and de la Peña [22]) and Ahuachapan (Ward and Jacobs [23]) suggest that geothermal anomalies are intimately associated with a specific pattern of faulting. For example, at East Mesa in the Imperial Valley of California, the Mesa fault is believed to act as conduit for the hot waters rising up from the depth (Combs and Hadley [24]). Bailey [25] hypothesized that the East Mesa geothermal reservoir owes its presence to the charging of hot waters from the fault at an intersection with an aquifer of sufficient horizontal permeability. The two dimensional conceptual model of such a system is shown in Fig. 1. The fault is considered to be a vertically oriented region, composed of highly fractured material of finite width ($2\,y'_e$). It extends downward through the interbedded sediments of the reservoir for a distance L' to the basement rock. At the surface, both the

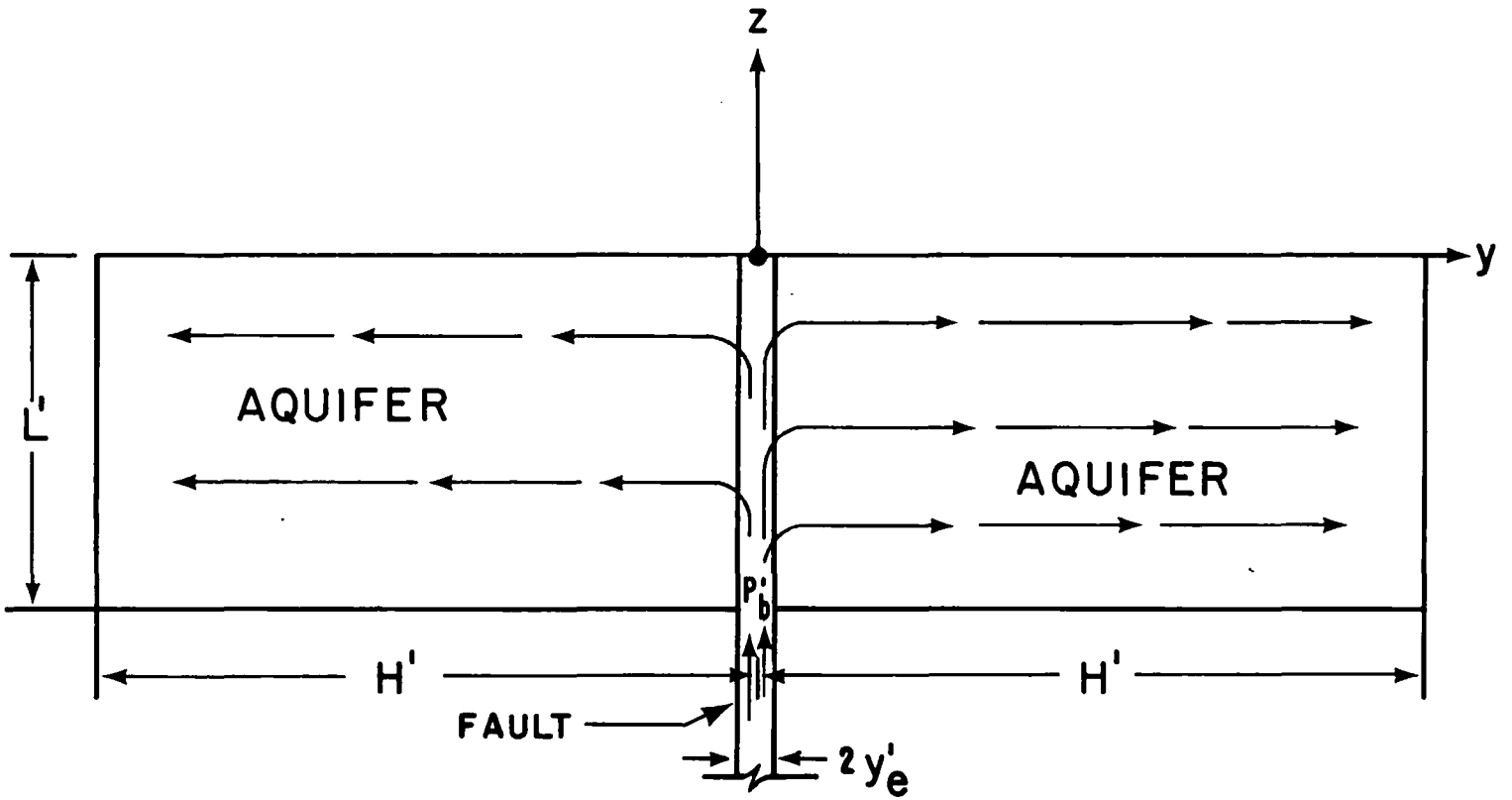

Fig. 1. Two-dimensional conceptual model of a liquid dominated geothermal reservoir.

reservoir and the fault are assumed overlain by a thin, impermeable, thermally conducting caprock. The depth of the reservoir (L') is assumed to be much larger than the fault width ($2 y_e'$). It is postulated that the fault is charged at depth by water which has been heated up in the fractured basement system. The mass flow rate or the pressure associated with the charging processes at the fault inlet cannot be known without a global analysis of the entire convection process. In the present analysis the pressure at the fault inlet at the bottom of the reservoir is considered to be a prescribed parameter. The hot, light liquid rises up in the reservoir section of the fault and is pushed into the aquifer due to the overpressure associated with the convection process. The liquid is assumed to flow only horizontally within the aquifer. Such a situation is believed to occur in some geothermal systems such as at East Mesa (Bailey [25]) and at Wairakei (I. G. Donaldson, personal communication, 1978), where the presence of shaly and sandy layers associated with interbedding reduce vertical transport in general.

For mathematical purposes the fracture zone is idealized as a vertical slab of homogeneous and isotropic porous material. The adjacent aquifer is represented as a porous medium of lateral half width H' with horizontal permeability much larger than the vertical value assumed to be of small absolute magnitude. Constant temperature boundary conditions are imposed at the hot bottom and cold top surfaces of the reservoir. At the vertical boundary far from the fault ($H' >> L' >> y_e'$) the temperature distribution is assumed to

be controlled by conduction, the pressure distribution is hydrostatic, and mass flux is required to conserve matter.

It is to be emphasized that this model is only a part of a "global circulation pattern." It does not define the downflow and heat up zones, and thus input mass or the pressures at the bottom of the fault are unknown. The driving mechanism for the convection, the result of a hydrostatic pressure imbalance between the hot upflow region and the cold downflow region, is identical to that envisioned by Donaldson [7].

MATHEMATICAL MODEL

A detailed derivation of the governing equations for a thermally active, saturated, deformable porous material is given in Goyal [16]. The equations used in the present study are obtained from the above by assuming that flow is steady, the solid matrix is rigid, the fault medium is homogeneous and isotropic, liquid properties are constant, the thermal conductivities of the fault and aquifer media are constant and equal, and that the vertical permeability in the aquifer is much smaller than the horizontal value, which is equal to that of the fault. Thus for all practical purposes vertical velocity in the aquifer is nearly zero. In addition, the Boussinesq approximation is invoked. The dimensional equations for the system shown in Fig. 1 and the related boundary and continuity conditions are given in the Appendix.

Within the fault, where the characteristic horizontal dimension and velocity component are much smaller than their vertical counterparts, appropriate nondimensional variables can be defined as:

$$\bar{y} = y'/y_e' \quad , \quad y_e = y_e'/L' \quad , \quad z = z'/L'$$

$$\bar{V} = V'/y_e q_o' \rho_o' \quad , \quad W = W'/q_o' \rho_o' \quad , \quad T = T'/T_o' \quad , \tag{1}$$

$$\tau = (T_{max}' - T_o')/T_o' \quad , \quad P = (P' - P_H')/p_o' \quad ,$$

where τ is defined as the overheat ratio and P as the overpressure which is in excess of hydrostatic pressure. Symbols with prime indicate a dimensional quantity while those without it denote a nondimensional quantity. Substitution of Eq. (1) into Eqs. (A1) to (A5) leads to an inherent balance between the buoyancy, Darcy flow, and pressure terms in the vertical momentum equation, if

$$q_o' = \frac{\alpha_e' \Delta T' g' K'}{\nu'} = \text{reference convection velocity}$$

$$p_o' = \rho_o' g' \alpha_e' L' \Delta T' = \text{reference convection pressure} \tag{2}$$

$$R = \frac{\rho_o' q_o' C_p' \Delta T'}{\lambda_m' (\Delta T'/L')} = \text{Rayleigh number}$$

where $\Delta T' = T_{max}' - T_o'$. The nondimensional equations, transformed boundary and continuity conditions relevant in the fault zone obtained by using Eqs. (1) and (2) in Eqs. (A1)-(A3), (A6), (A7) and (A10b) can be written as

Fault Zone:

$$\bar{V}_{\bar{y}} + W_z = 0 \quad ; \quad y_e^2 \bar{V} = -P_{\bar{y}} \quad ; \quad W = -P_z + (T - 1)/ \tag{3a-c}$$

$$\gamma^2 (\bar{V} T_{\bar{y}} + W T_z) = T_{\bar{y}\bar{y}} + y_e^2 T_{zz} \quad ; \quad \gamma = R^{1/2} y_e \tag{4a,b}$$

$$W(\bar{y},0) = 0 \quad ; \quad P(\bar{y},-1) = P_b \quad ; \quad P_b = (P_b' - P_H')/p_o' \qquad (5a\text{-}c)$$

$$T(\bar{y},0) = 1 \quad ; \quad T(\bar{y},-1) = 1 + \tau \; ; \quad T_{\bar{y}}(0,z) = 0 \quad ; \quad \bar{V}(\pm 1,z) = \pm v(z) \qquad (6a\text{-}d)$$

For the aquifer, within which the horizontal scale is measured by $\hat{y} = y'/H'$, the pressure $p = P$, the temperature $\theta = T$, and the velocity $v = \bar{V}$, the appropriate system of equations obtained from Eqs. (A4) and (A5) is given by:

Aquifer:

$$v(z) = -p_{\hat{y}}/d \quad ; \quad d_\gamma^2 v(z)\, \theta_{\hat{y}} = y_e^2 \theta_{\hat{y}\hat{y}} + d^2 \theta_{zz} \qquad (7a,b)$$

where

$$H'/L' = d/y_e \quad , \quad d = O(1) \text{ number} \qquad (8a,b)$$

The magnitude of H' with respect to the fault depth, L', given in Eq. (8a) is chosen to ensure a balance between the nondimensional aquifer velocity v and the horizontal pressure gradient as shown in Eq. (7a). The number d, used in this study to define the location of the far field boundary of the aquifer, will be determined during the course of this paper. It is assumed that the hot liquid loses its heat to the surroundings to the extent that the horizontal temperature gradient becomes vanishingly small far from the fault. It may be emphasized that horizontal motion exists at the far field boundary but that heat transfer is due to vertical conduction only. The related boundary conditions as obtained from Eqs. (A8), (A10a) and (A9) are:

$$\theta(\hat{y},0) = 1 \quad ; \quad \theta(\hat{y},-1) = 1 + \tau \qquad (9a,b)$$

$$\theta(\hat{y} = y_e^2/d, z) = T(\bar{y} = 1, z) \quad ; \quad \theta(\hat{y}=1, z)\ 1 - \tau z \qquad (10a,b)$$

In order to proceed further we must consider the magnitude of the Rayleigh number and the parameter γ. If parameter values typical of geothermal systems ($K' = 10^{-13}$ m^2 and thermodynamic variables evaluated at $T_0' = 298$ K) are used in Eq. (1) and (2) we find that

$$3 \times 10^5 \text{ Pa} \leq p_0' \leq 15 \times 10^5 \text{ Pa}$$

$$10^{-2} \text{ m/day} \leq q_0' \leq 10^{-1} \text{ m/day}$$

$$0.2 \leq \tau \leq 1$$

$$2 \times 10^2 \leq R \leq 10^4$$

Large values of R suggest that energy transfer associated with liquid convection is far greater than that due to conduction. In this regard one may expect that fluid particles moving through the system will tend to behave isothermally unless affected by cooling associated with a relatively cold boundary.

The parameter γ is assumed to be an O(1) number because y_e is considered small. If, for instance, we consider $R = 10^3$ and $L' = 2$ km then $y_e' = 63.2\ \gamma$ meters, indicating that reasonable fault zone thicknesses can be incorporated in the theory. In the mathematical analysis solutions are sought in the limit of large R with $\gamma = O(1)$ implying, of course that y_e is small.

The cooling effect of the surface is confined to a thin thermal boundary layer near the top of the fault for a high Rayleigh number flow. The temperature of the fluid changes from $1 + \tau$ to 1 in the boundary layer due to heat loss to the upper cold boundary. The thickness of the boundary layer increases as fluid moves away from the fault due to increased heat loss. The boundary layer virtually occupies the whole depth of the aquifer in the far field. Thus, the flow outide the boundary layer is an isothermal flow.

It can be noted from Eq. (3b) that the horizontal pressure gradient in the fault is very small, $O(y_e^2)$. Thus, the basic fault pressure is only a function of depth and can be calculated in terms of W and v. The horizontal aquifer velocity v(z) can then be calculated explicitly from Eq. (7a) because the far field pressure is known, once Eq. (10b) is specified. Upon decoupling the fluid mechanics from the thermal problem, the energy Eq. (7b) can then be solved for the temperatures in the aquifer.

FAULT ZONE SOLUTION

The water in the fault zone rises up adiabatically because the convection Rayleigh number is considered to be large. Even the liquid in the aquifer just adjacent to the fault remains at the supply temperature. Cooling in the fault itself can take place only in a thin boundary layer just below the cold upper surface. The uppermost portion of the neighboring aquifer is similarly affected.

The basic solutions in the isothermal portions of the fault and aquifer system are:

$$T = 1 + \tau \tag{11}$$

$$\bar{V} = \bar{y}\left[\frac{C_1}{d}\cosh z/\sqrt{d} + b_1 \sinh z/\sqrt{d} - 1\right] + O(y_e^2) \tag{12}$$

$$W = -\frac{C_1}{\sqrt{d}}\sinh z/\sqrt{d} - \cosh z/\sqrt{d} + z + 1 + O(y_e^2) \tag{13}$$

$$P = d\left\{\frac{C_1}{d}\cosh z/\sqrt{d} + b_1 \sinh z/\sqrt{d} - 1\right\} - z^2/2 + O(y_e^2) \tag{14}$$

$$v(z) = \frac{C_1}{d}\cosh z/\sqrt{d} + b_1 \sinh z/\sqrt{d} - 1 + O(y_e^2) \tag{15}$$

$$p = v(z)\, d(1 - \hat{y}) - z^2/2 + O(y_e^2) \tag{16}$$

where

$$C_1 = \frac{P_b + d + \frac{1}{2} + \sqrt{d}\sinh\frac{1}{\sqrt{d}}}{\cosh\frac{1}{\sqrt{d}}} \quad , \quad b_1 = \frac{1}{\sqrt{d}} \tag{17a,b}$$

It can be noted that $(-z^2/2)$ is the pressure at the far field boundary of the aquifer and is consistent with the specified temperature field (Eq. (10b)).

According to Eq. (6a), the nondimensional temperature at the top of the fault is 1. There should be a boundary layer to accommodate the temperature drop from $1 + \tau$ to 1. If the appropriately scaled variables

$$\bar{z} = z/y_e \quad \text{and} \quad \bar{W} = W/y_e \tag{18a,b}$$

are used in the basic fault-zone Eq. (3) and (4a) then the lowest order boundary layer system has the form:

$$V_{o\bar{y}} + W_{o\bar{z}} = 0 \tag{19}$$

$$P_{1\bar{y}} = 0 \quad ; \quad \frac{T_o - 1}{\tau} - P_{1\bar{z}} = 0 \tag{20a,b}$$

$$\gamma^2(V_o T_{o\bar{y}} + W_o T_{o\bar{z}}) = T_{o\bar{y}\bar{y}} + T_{o\bar{z}\bar{z}} \tag{21}$$

However, it can easily be seen that the lowest order fault pressure P_o is a constant and when matched with the outer solution Eq. (14) one finds that

$$P_o = C_1 - d \tag{22}$$

The solution to the system of Eqs. (19) and (21) is subjected to the following boundary, matching and continuity conditions.

$$T_o(\bar{y},0) = 1 \quad ; \quad T_o(\bar{y},\bar{z} \to -\infty) = 1 + \tau \tag{23a,b}$$

$$W_o(\bar{y},\bar{z} \to 0) = 0 \quad ; \quad W_o(\bar{y},\bar{z} \to -\infty) = -\bar{z} - 1 + \frac{C_1}{d} \tag{24a,b}$$

$$V_o(\bar{y},\bar{z} \to -\infty) = \frac{C_1}{d} - 1\ \bar{y} \quad ; \quad P_1(\bar{y},\bar{z} \to -\infty) = \bar{z} \tag{25a,b}$$

It can be noted that the matching conditions ($\bar{z} \to -\infty$) are obtained from the outer solutions (Eqs. (11-14)). The boundary layer solutions can be written as:

$$\bar{V} = \left(\frac{C_1}{d} - 1\right)\bar{y} + O(y_e) \quad , \quad \bar{W} = -\left(\frac{C_1}{d} - 1\right)\bar{z} + O(y_e) \tag{26a,b}$$

$$T = 1 - \tau\ \mathrm{erf}(A\bar{z}) + O(y_e) \tag{27}$$

$$P = d\left[\frac{C_1}{d} - 1\right] - y_e\left\{\bar{z}\ \mathrm{erf}(A\bar{z}) + \frac{1}{A\sqrt{\pi}}\ e^{-A^2\bar{z}^2}\right\} + O(y_e^2) \tag{28}$$

where

$$A = \sqrt{\gamma^2\left(\frac{C_1}{d} - 1\right)\Big/2} \tag{29}$$

The thermal boundary layer initiated at the top of the fault continues into the adjacent aquifer over a horizontal distance of scale y_e'. In this initial aquifer zone of water cooling, the relevant equation for the velocity and pressure field as obtained from Eq. (7a) is

$$v_o(\bar{z}) = -p_{o\hat{y}}/d \tag{30}$$

The appropriate matching and continuity conditions as obtained from Eqs. (6d), (15) and (16) are expressed as:

$$V_o(\pm 1, \bar{z}) = \pm v_o(\bar{z}) \quad ; \quad v_o(\bar{z} \to -\infty) = \frac{C_1}{d} - 1 \tag{31a,b}$$

$$p_o(\hat{y}, \bar{z} \to -\infty) = d(1 - \hat{y})\left(\frac{C_1}{d} - 1\right) \tag{32}$$

The solution forms are given by

$$v(\bar{z}) = \left(\frac{C_1}{d} - 1\right) + O(y_e) \quad ; \quad p(\hat{y},\bar{z}) = d\left(\frac{C_1}{d} - 1\right)(1 - \hat{y}) + O(y_e) \quad (33a,b)$$

TEMPERATURE DISTRIBUTIONS WITHIN THE AQUIFER

Once the velocity field in the aquifer is known, the temperature can be calculated from the energy equation. This must be done for five different regions shown in Fig. 2. In the near field, where length scale is of $O(y_e')$, the aquifer energy equation, as obtained by using Eqs. (1), (8a) and (18a) in Eq. (7b), can be written as follows for region 1:

$$\gamma^2 v(\bar{z})\, \theta_{\bar{y}} = \theta_{\bar{y}\bar{y}} + \theta_{\bar{z}\bar{z}} \quad (34)$$

Equation (7b) takes the following form to describe the thermal boundary layer in region 3

$$\gamma^2 v(z^*)\, \theta_y = y_e \theta_{yy} + \theta_{z^*z^*} \quad (35)$$

where

$$y = y'/L' \text{ and } z^* = z/y_e^{1/2} \quad (36a,b)$$

Since the effect of the surface cooling is limited to the boundary layer regions 1 and 3, the flow in regions 2 and 4 is isothermal. The energy equation in the far field where the full depth of the aquifer

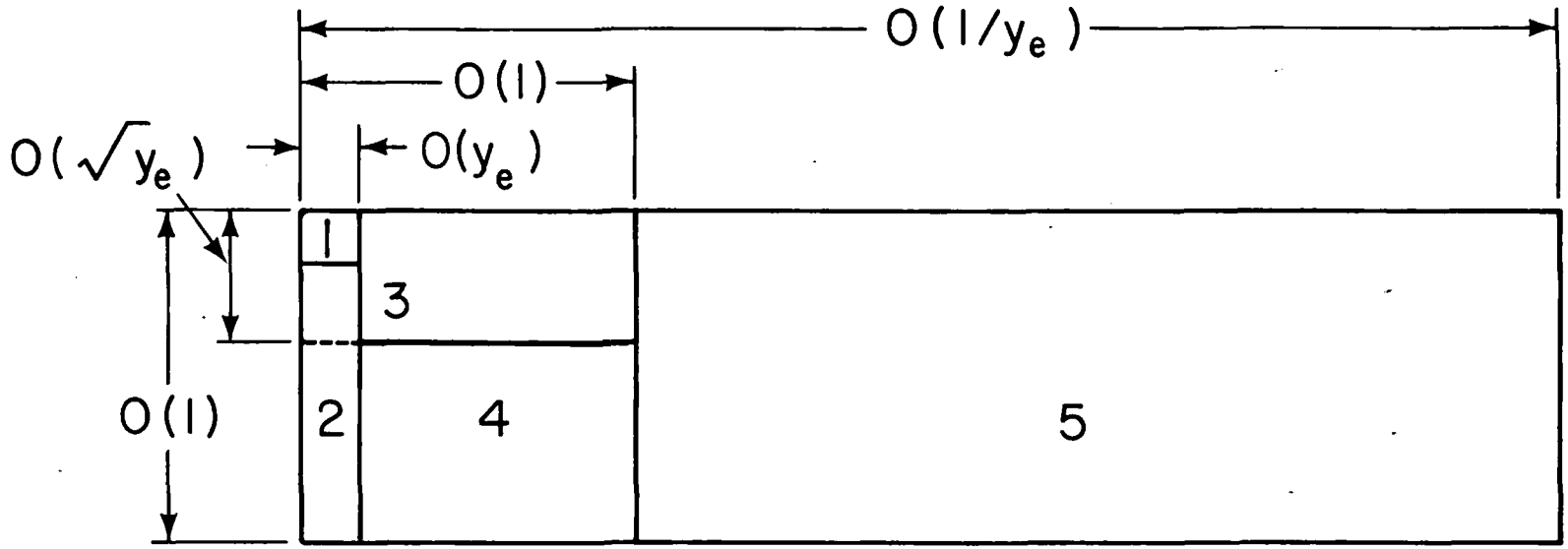

Fig. 2. Five different regions in the aquifer.

is affected by the surface cooling is expressed in terms of $\hat{y}$ and z and is given by Eq. (7b).

Equation (34) is subjected to the following boundary conditions.

$$\theta(1,\bar{z}) = T(1,\bar{z}) = 1 - \tau \operatorname{erf}(A\bar{z}) \quad ; \quad \theta(\bar{y}\to\infty,\bar{z}) \text{ bounded} \qquad (37a,b)$$

$$\theta(\bar{y},0) = 1 \quad ; \quad \theta(\bar{y},\bar{z}\to -\infty) = 1 + \tau \qquad (38a,b)$$

Equation (37a) represents the continuity of the temperature at the interface between the fault and the aquifer as found in Eq. (27). The solution in region 1 can be written as

$$\theta(\bar{y},\bar{z}) = 1 - \frac{2\tau}{\pi}\int_{-\infty}^{0} \exp\left\{-\frac{\omega^2}{4A^2} - A^2 + \sqrt{A^4 + \omega^2}\right.$$

$$\left. + (A^2 - \sqrt{A^4 + \omega^2})\,\bar{y}\right\} \frac{\sin \omega\bar{z}}{\omega}\, d\omega \qquad (39)$$

by using the Fourier sine integral transform of θ with respect to $\bar{z}$. When $\bar{y} \to \infty$, the asymptotic form of Eq. (39) is

$$\theta(\bar{y},\bar{z}) = 1 - \sqrt{2}/\pi\ \tau A\bar{z}/\bar{y}^{1/2} \qquad (40)$$

which indicates that a similarity variable $z/y^{1/2}$ will be significant in region 3. The thermal boundary layer in the latter region is born in the preceding elliptic region as described formally in Eckhaus (26).

A similarity solution, compatible with the solution in region 1 can be obtained in the region 3. Elementary methods yield

$$\theta(y,z^*) = 1 - \operatorname{erf}\left(\frac{A}{\sqrt{2}}\,\eta\right), \quad \eta = z^*/y^{1/2} \tag{41a,b}$$

It is possible to obtain an analytical solution of Eq. (7b) in region 5, when $\hat{y} << 1$ and $z << 1$, such that $z/\hat{y}^{1/2} = O(1)$, which can be matched with Eq. (41a). We find the form

$$\theta(\hat{y},z) = 1 - \tau \operatorname{erf}\left[\frac{A}{\sqrt{2d}}\,\frac{z}{\hat{y}^{1/2}}\right] + \frac{\hat{y}^{1/2}\,\tau\gamma^2}{4\sqrt{2d}\,A^2}\left[\frac{z}{\sqrt{2d\hat{y}}}\left\{1 + \operatorname{erf}\left(\frac{Az}{\sqrt{2d\hat{y}}}\right)\right\} - \frac{Az^2}{d\hat{y}\sqrt{\pi}}\,e^{-\frac{A^2z^2}{2d\hat{y}}}\right] + O(\hat{y}) \tag{42}$$

by using coordinate expansion methods. This solution provides the transition between the incompatible conditions $\theta(\hat{y},0) = 1$, $\theta(\hat{y}>0,z) = 1 + \tau$ for $|z| > 0$ in the vicinity of the singular corner $\hat{y} = z = 0$.

The energy equation in Eq. (7b), parabolic to the lowest order, must be solved subject to the boundary conditions in Eqs. (9a) and (9b) and the initial condition $\theta(\hat{y}>0,z) = 1 + \tau$ for $|z| > 0$ obtained from matching with region 4. The last formal condition at the far end of the aquifer, Eq. (10b), is used to determine a value for d. Numerical integration by standard finite difference methods is carried out for assumed values of d until the solution at the far edge is within 0.5 percent of the real condition. This approximation provides an engineering-type estimate of the boundary location. At that point convection of energy associated with the $\theta_{\hat{y}}$ -term in Eq. (7b) is very small compared to the conduction term. Of course in the formal mathematical sense, the purely conductive profile can be found only

for $\hat{y} \to \infty$. From the mathematical viewpoint, the reduction of the full-elliptic problem in the far-field aquifer to the parabolic system in Eq. (7b) permits a simplified numerical computation procedure. The fact that the reduction can be developed in a formal, rational manner for the large Rayleigh number approximation shows that the imposition of the far field boundary condition at an a priori specified location is fundamentally unsound. In physical terms, this implies that the thermal anomaly associated with the upward fault zone flow has a natural horizontal relaxation length, associated basically with the distance required to transfer out of the surface, heat in excess of that arising from the natural geothermal gradient $\Delta T'/L'$. A quantitative indication of this matter involves the evaluation of d.

It is found that d is different for different sets of parameters as listed in Table 1. It can be observed from this table that an increase in P_b, R, or y_e increases d; which means that a larger aquifer is needed for the transition to the conduction temperature profile when the parameter is increased. In physical terms this result implies that the hot isothermal portions of the aquifer, maintained by horizontal convection effects will be more extensive in systems of relatively larger fault inlet pressure, permeability and fault size.

RESULTS AND DISCUSSION

The analysis carried out in the preceding sections should be applied for a range of parameters which is representative of typical geothermal systems. Goyal and Kassoy [17] calculated a Rayleigh number (R) of 338, over heat ratio (τ) of 0.6 and semi fault width

(y_e) of 0.034 for the East Mesa geothermal field in the Imperial Valley of California. Accordingly, the following parameters representative of a typical geothermal system are selected in our calculations

$$R = 500 \quad , \quad \tau = 1 \quad , \quad y_e = 0.025$$

The dependence of various parameters on the velocity, pressure, temperature and surface heat flux in the fault and the aquifer is given in Figs. 3 to 23. The value of d used in these figures is for the parameters shown.

Figure 3 shows the vertical velocity (W) in the fault as obtained from Eq. (13) at various depths for different inlet pressures (P_b). It may be noted that an increase in the inlet pressure leads to an increase in the vertical velocity. It is consistent with the commonly held notion that one would require higher pressure to push more mass into the system. The vertical velocity vanishes at the top of the fault due to the impermeable boundary assumption. All the water is pushed to the aquifer by the time it reaches the top surface of the fault.

Figure 4 shows the effect of Rayleigh number on the nondimensional vertical velocity in the fault as obtained from Eq. (13). It may be noted that an increase in Rayleigh number reflects a decrease in nondimensional vertical fault velocity (W). In physical terms an increase in R is equivalent to an increase in the reference convection velocity q_o' as shown in Eq. (2). Thus, in fact, what we see in figure 4 is

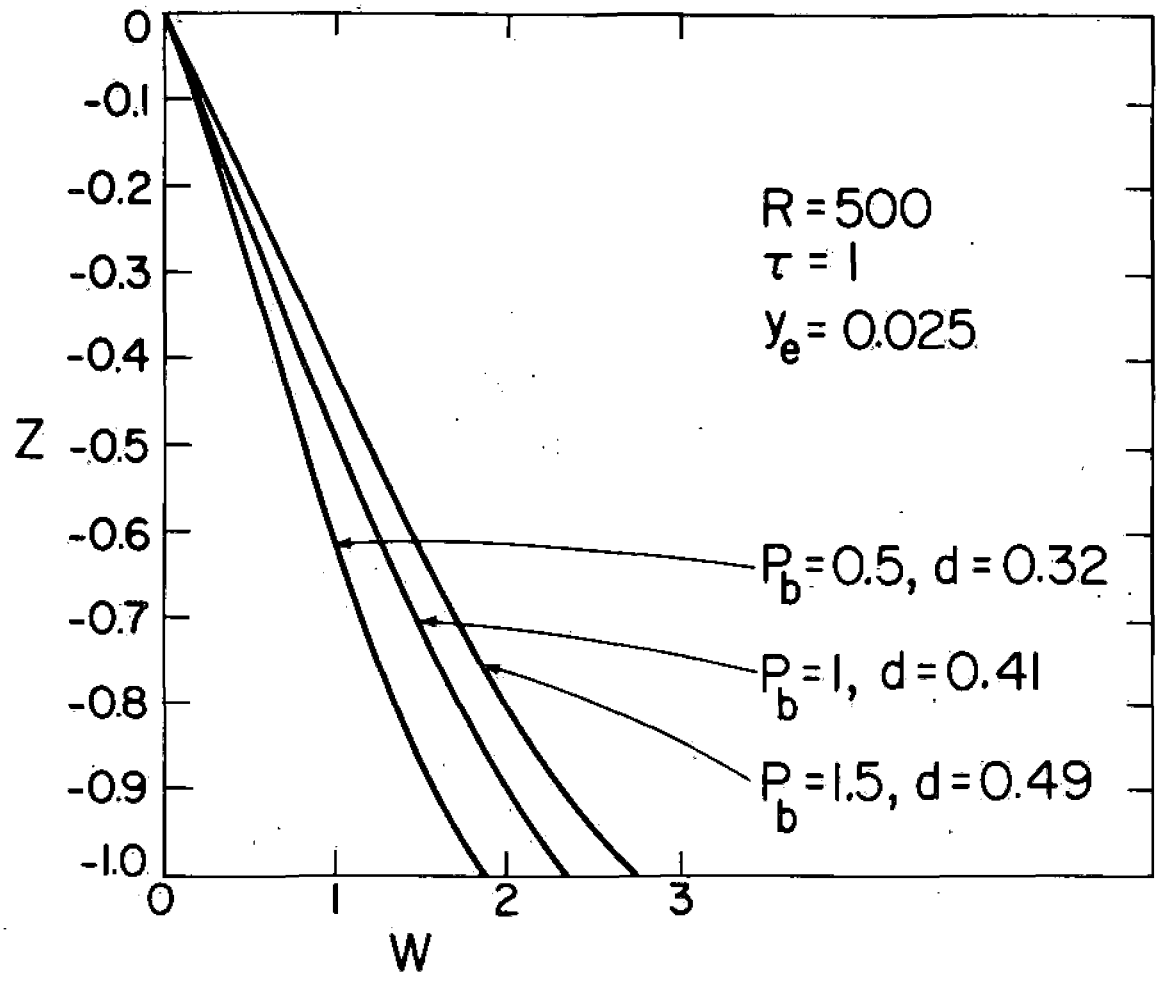

XBL 8011-2369

Fig. 3. Vertical velocity distributions along the depth of the fault for various values of P_b.

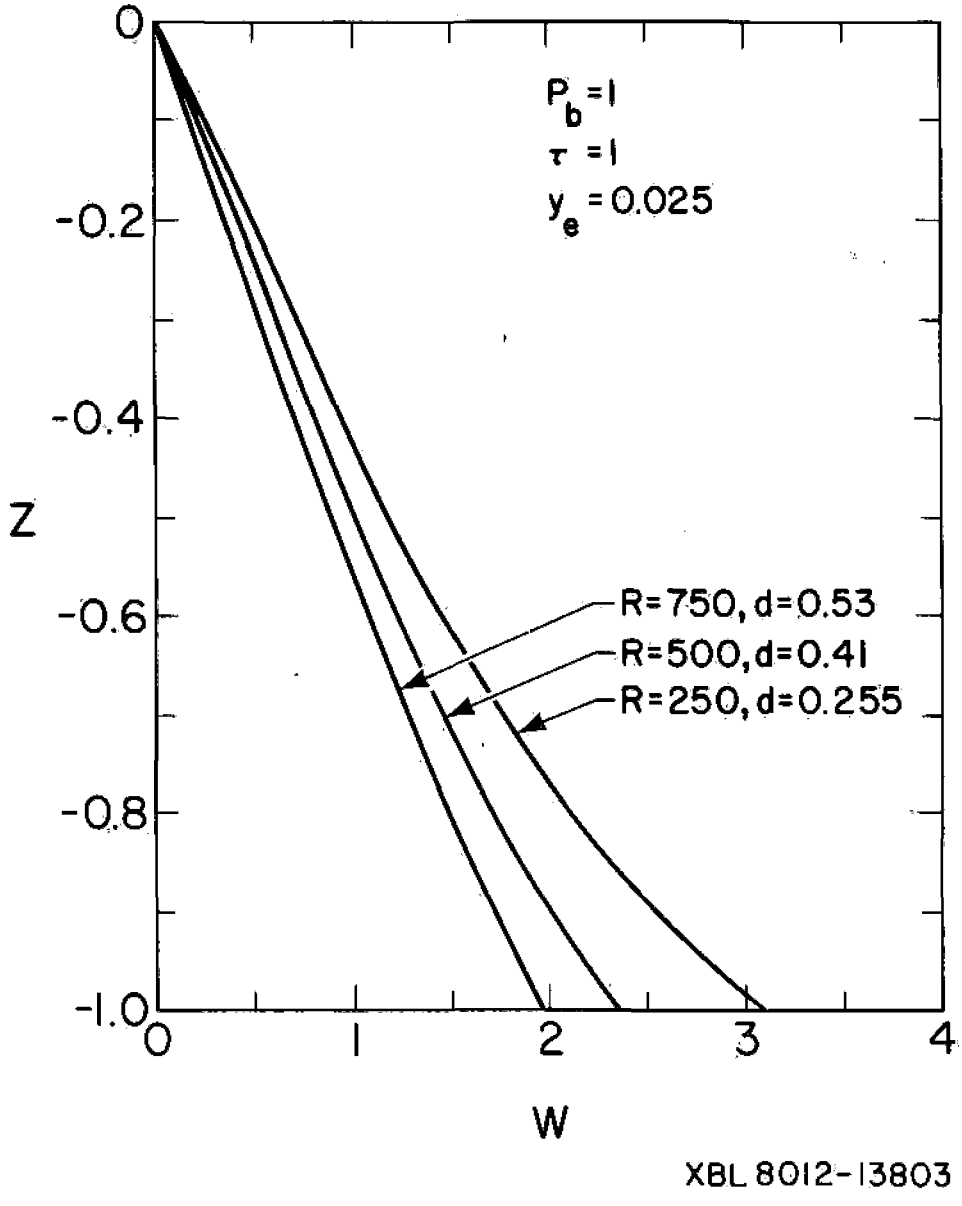

Fig. 4. Effect of Rayleigh number on the vertical velocity in the fault.

that the dimensional vertical velocity (W') in the fault increases for higher Rayleigh number. It is verified by calculating dimensional vertical velocity (W') in the fault for various reference convection velocities (q_o') associated with Rayleigh numbers shown in Fig. 4. This increase in W' with increased R is consistent with the general belief that an increase in Rayleigh number leads to improved convection effects.

Figure 5 is a plot of non-dimensional vertical fault velocity (W) versus depth for different values of semi fault width y_e. For a given P_b, vertical velocities in the fault decrease with increasing y_e. It has been verified that the total dimensional mass influx (M') to the system is higher for increased inlet area associated with higher value of y_e. However, for a prescribed P_b, an increase in M' is not found to be proportional to that in the area, but, in fact a smaller increase in mass flux is observed, giving rise to lower vertical velocities as shown in this figure. The added heat, associated with increased mass input would require a longer aquifer to cool off to the conduction profile. It is supported by the increased value of d for $y_e = 0.05$ as shown in figure 5.

Figure 6 is a plot of fault overpressure (P) versus depth for different values of P_b as computed from Eq. (14). As one may expect, the overall fault pressures increase for an increased inlet pressure (P_b). Note that the fault pressures decrease upwards and then increase toward the top of the fault. This increase toward the top is caused by the stagnation point at $z = 0$.

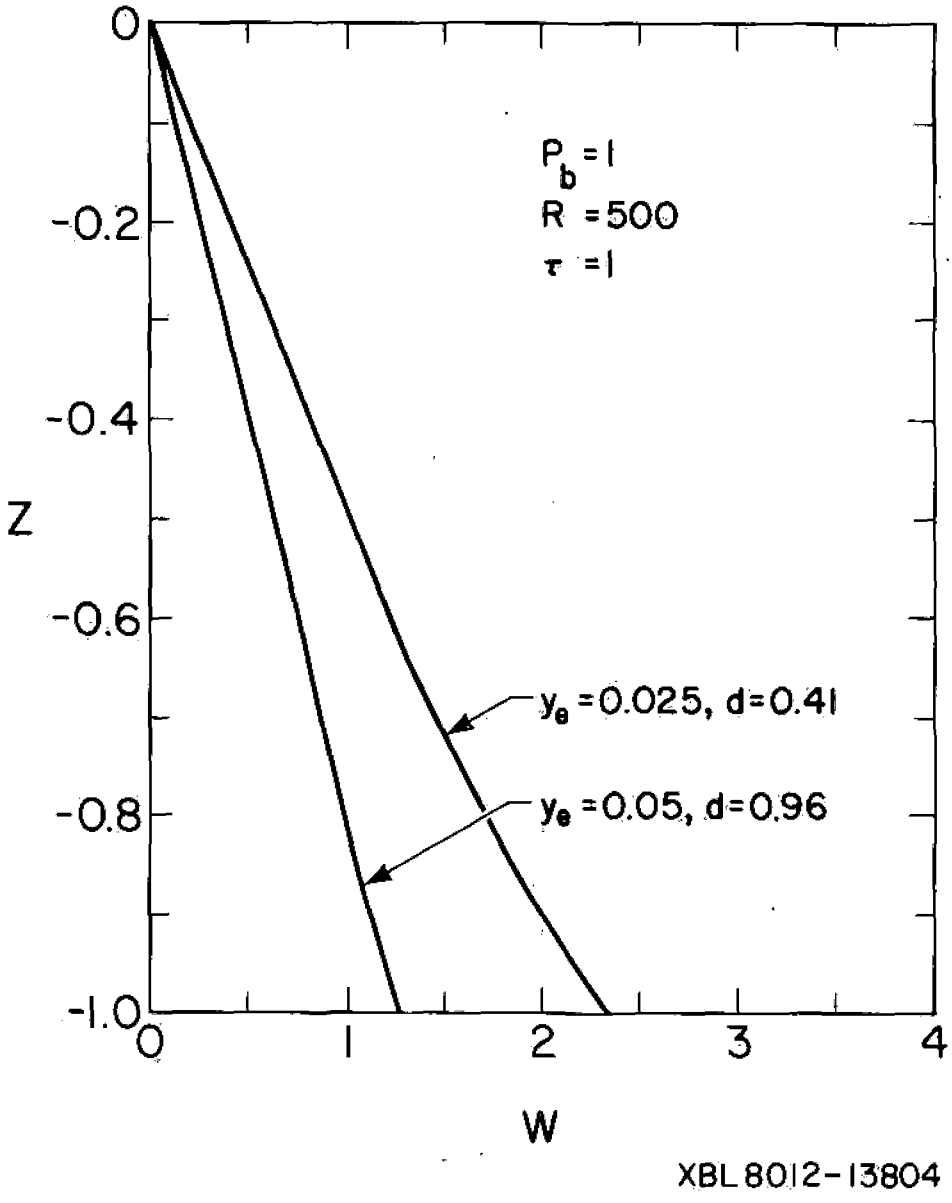

Fig. 5. Vertical velocity in the fault versus depth for different fault widths.

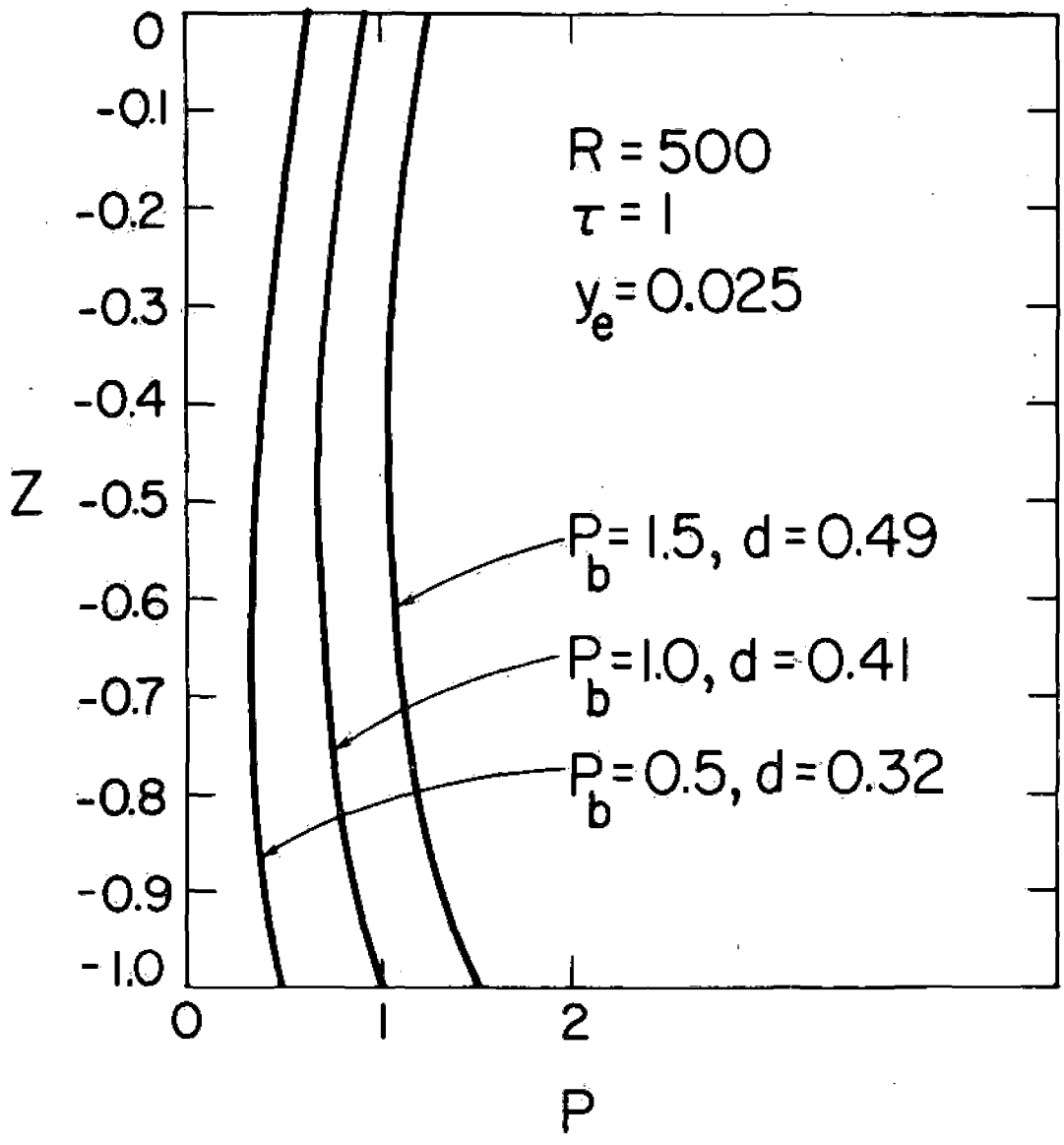

XBL 8011-2370

Fig. 6. Fault overpressures versus depth for various values of P_b.

A plot of fault overpressure versus depth, as calculated from Eq. (14), is shown in Fig. 7 for various values of Rayleigh numbers. Fault overpressures rise for increased values of R. Increased convection effects associated with higher Rayleigh numbers would tend to enhance the pressures in the fault as shown in this figure.

The effect of semi fault width on the fault overpressures is shown in Fig. 8. Fault overpressures increase for higher values of y_e. As discussed in Fig. 5, the dimensional mass influx to the system increases with higher values of y_e, requiring higher fault pressures to sustain the increased mass flux. Alternatively lower W associated with higher y_e in Fig. 5 would tend to reduce the vertical pressure gradient in the fault resulting into higher fault-pressures as shown in Fig. 8.

The fluid temperatures in the fault are shown in Fig. 9 for various values of P_b as obtained from Eq. (27). Higher vertical velocities associated with increased P_b give rise to higher temperatures as indicated in the figure. Only 12 percent of the total depth of the fault, representing the boundary layer, is shown in this figure. The temperature drop from $1 + \tau$ to 1, due to heat loss to the surroundings, takes place in the upper 8 percent of the fault depth indicating the generation of a thin thermal boundary layer at the top of the fault. The temperatures in the lower 90 percent of the fault are constant and equal to the highest temperature value of $1 + \tau$. It may be worth mentioning here, that an increase in P_b from 0.5 to 2.0 does not increase the specified dimensional pressure by four times but only by a small

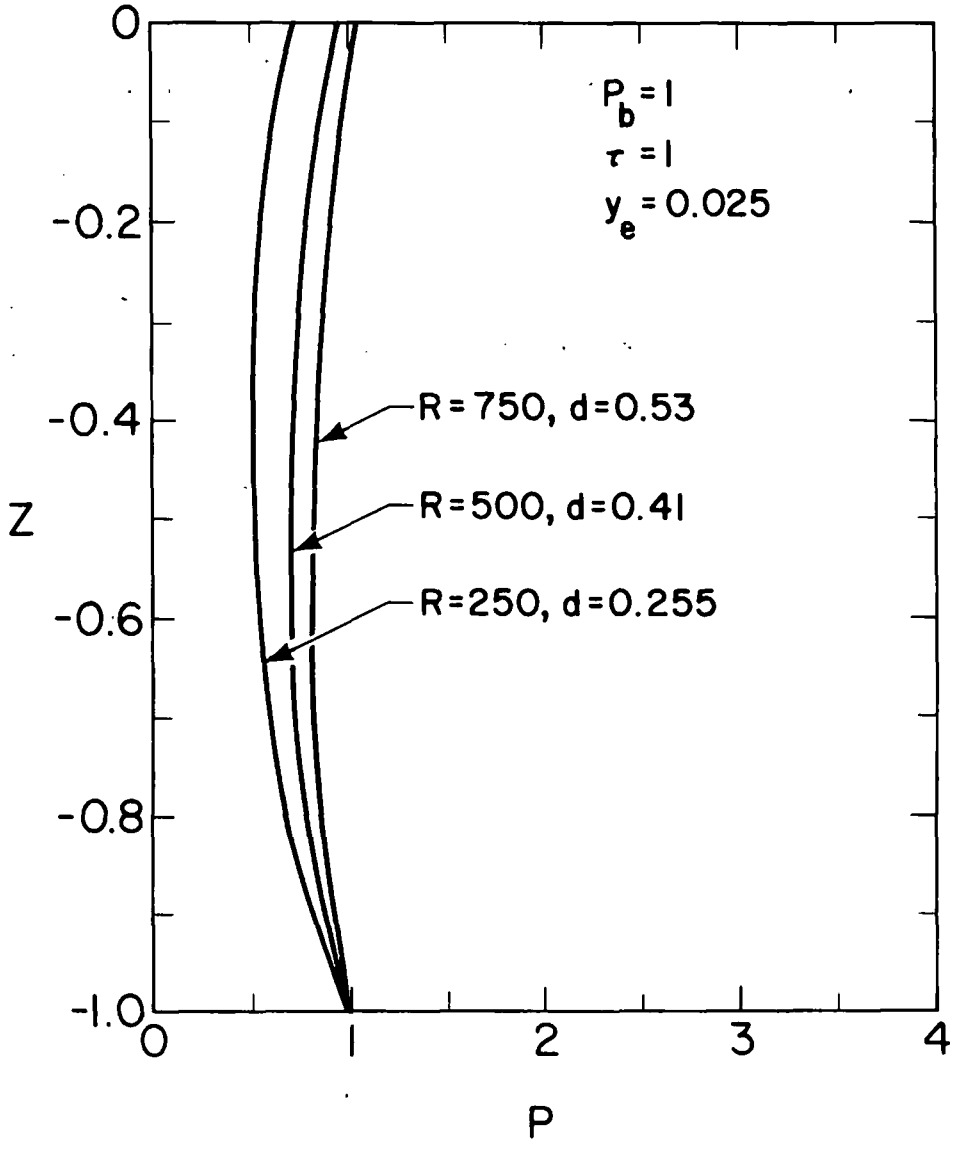

Fig. 7. Effect on Rayleigh number on the fault overpressure.

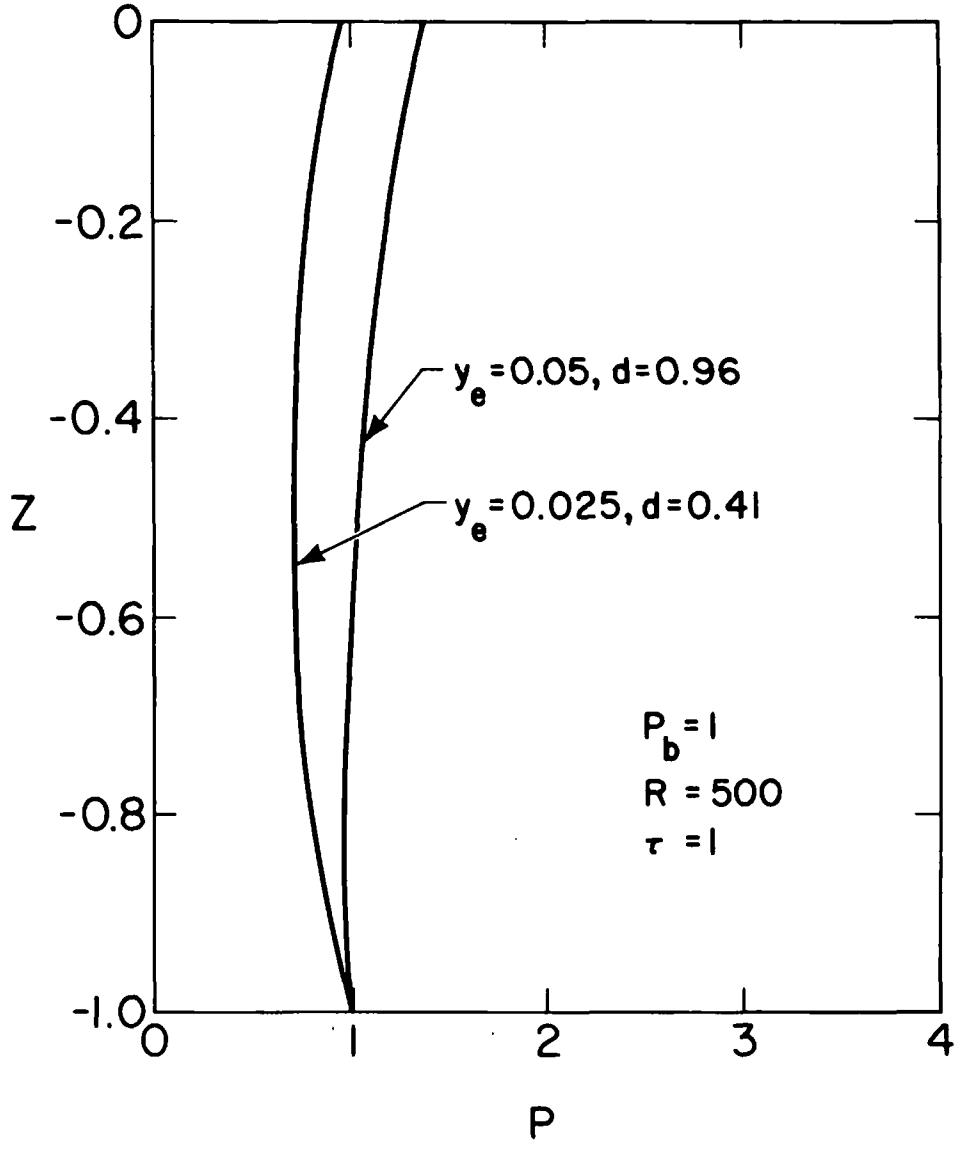

Fig. 8. Fault overpressures versus depth for different values of y_e.

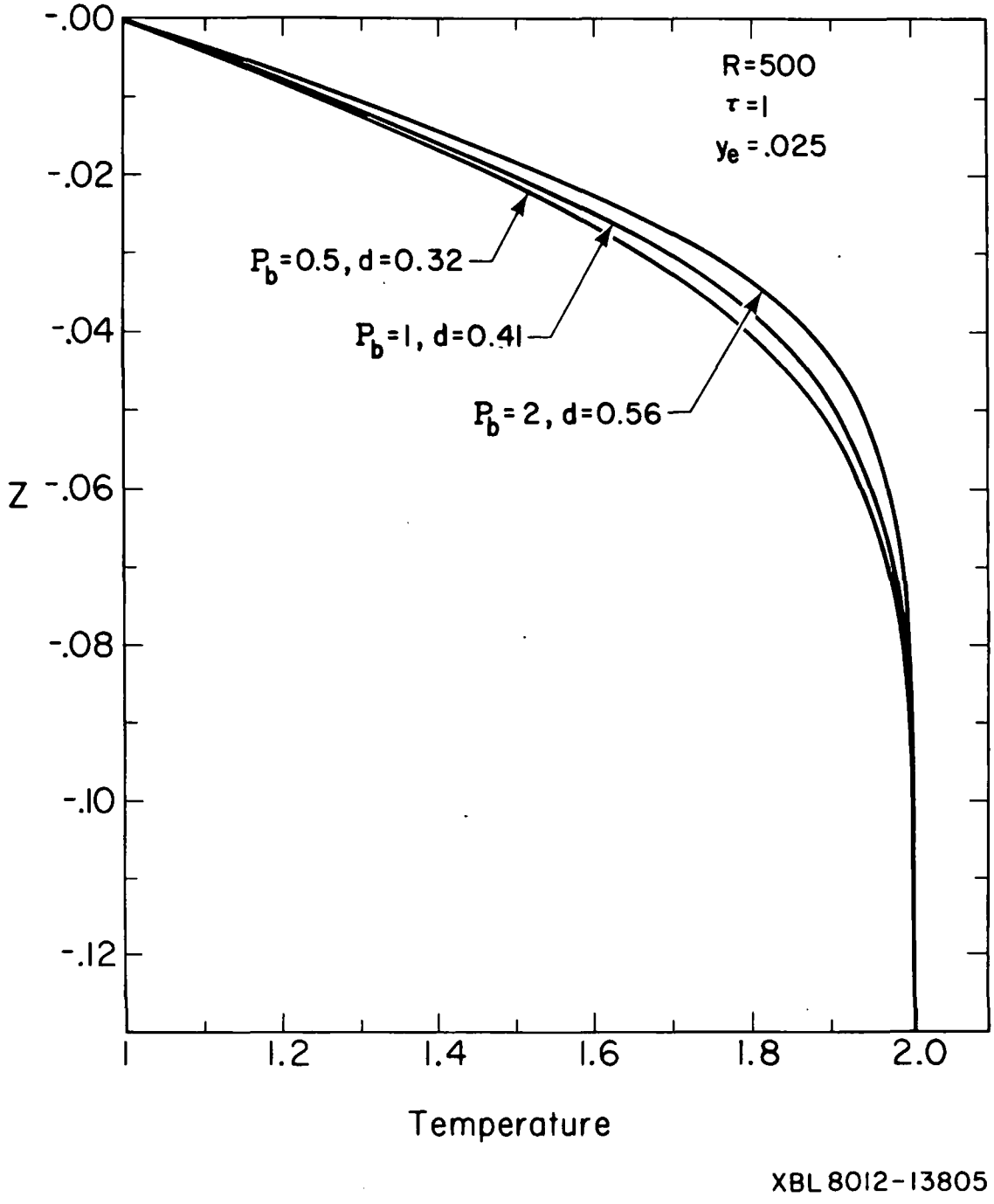

Fig. 9. Fluid temperatures in the fault for various values of P_b.

fraction. For example, P_b equal 0.5, 1 and 2 represent about 297,300 and 307 bars respectively, if we use the typical reservoir data discussed on page 50 of this report.

Figure 10 contains a plot of temperature versus depth for various values of Rayleigh number in the upper 12 percent of the fault. Temperatures in the thin thermal boundary layer at the top of the fault rise with an increase in the Rayleigh number or alternatively, the thickness of the boundary layer decreases with increased R. This increase is caused due to enhanced convection effects associated with higher R as discussed in Figs. 4 and 7.

The effect of semifault width (y_e) on the boundary layer temperature in the fault, obtained from Eq. (27), is shown in Fig. 11. Boundary layer temperatures are seen to decrease with increasing y_e. This decrease is caused by reduced convection effects due to lower vertical velocity in the fault associated with increased fault width as discussed in Fig. 5.

The horizontal velocity in the aquifer calculated from Eq. (15) at various depths is shown in Fig. 12 for different inlet pressures. As expected, horizontal aquifer velocities increase for an increased inlet pressure. The trend of the curves is similar to the overpressure curves in Fig. 6. The larger velocities at the top of the aquifer are associated with the relatively higher horizontal pressure gradients there.

The effect of Rayleigh number on the horizontal velocity in the aquifer is shown in Fig. 13. The nondimensional horizontal velocity in the aquifer decreases with increasing R. It may be noted that the

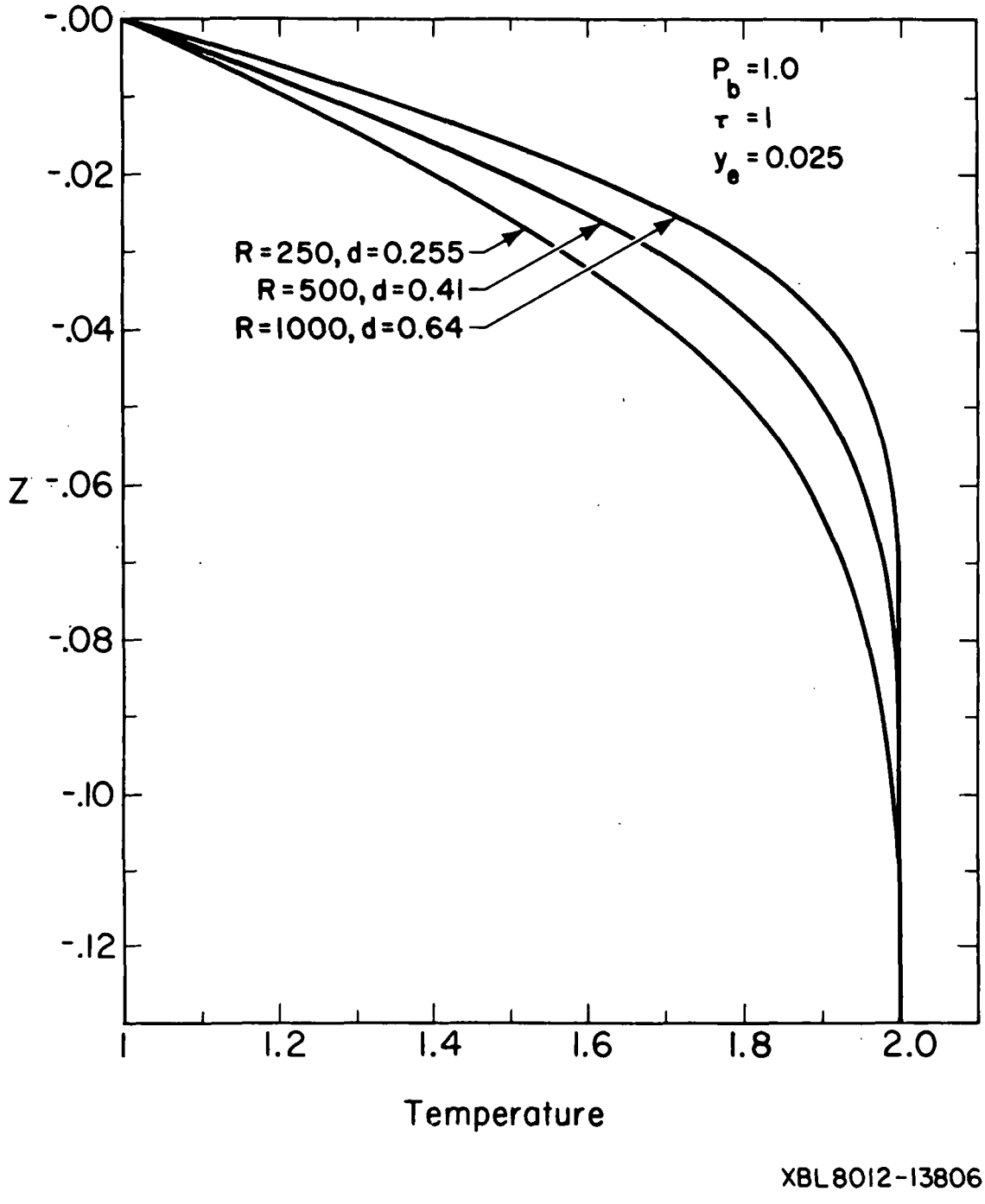

Fig. 10. Fluid temperatures in the fault versus depth for various values of R.

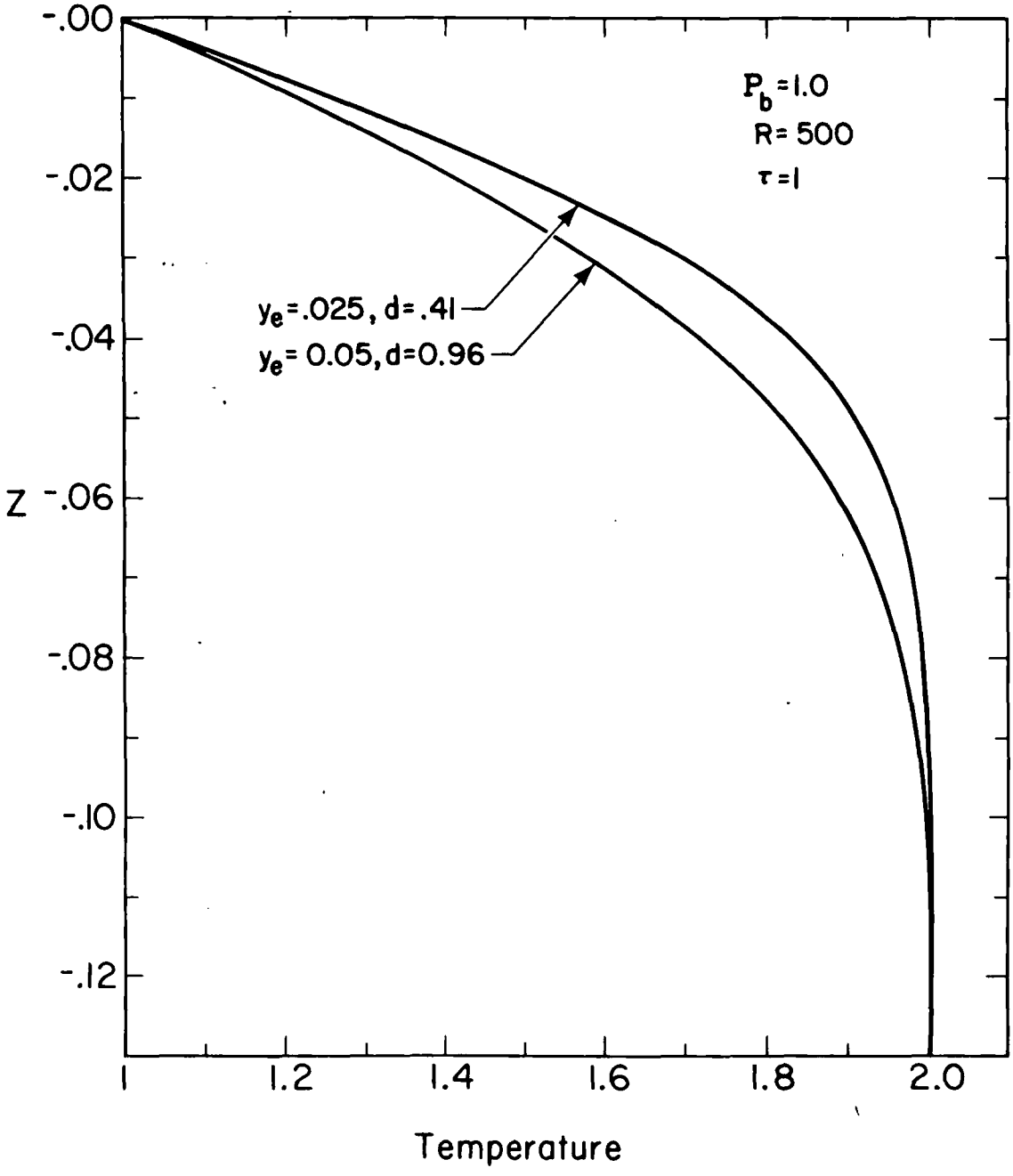

XBL 8012-13807

Fig. 11. Effect of semifault width on the boundary layer temperatures in the fault.

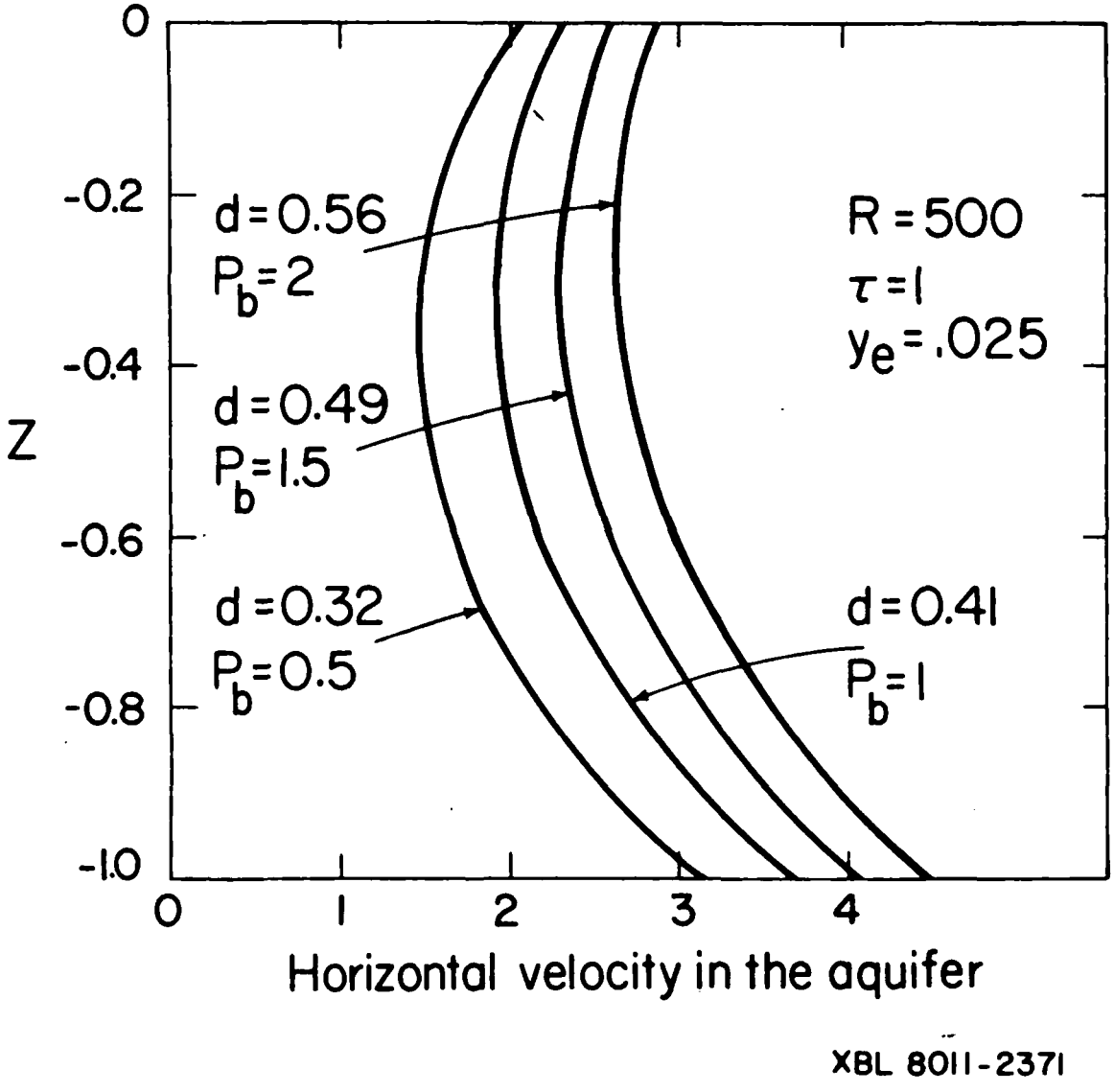

Fig. 12. Nondimensional horizontal liquid velocity in the aquifer along the depth of the reservoir for different values of P_b.

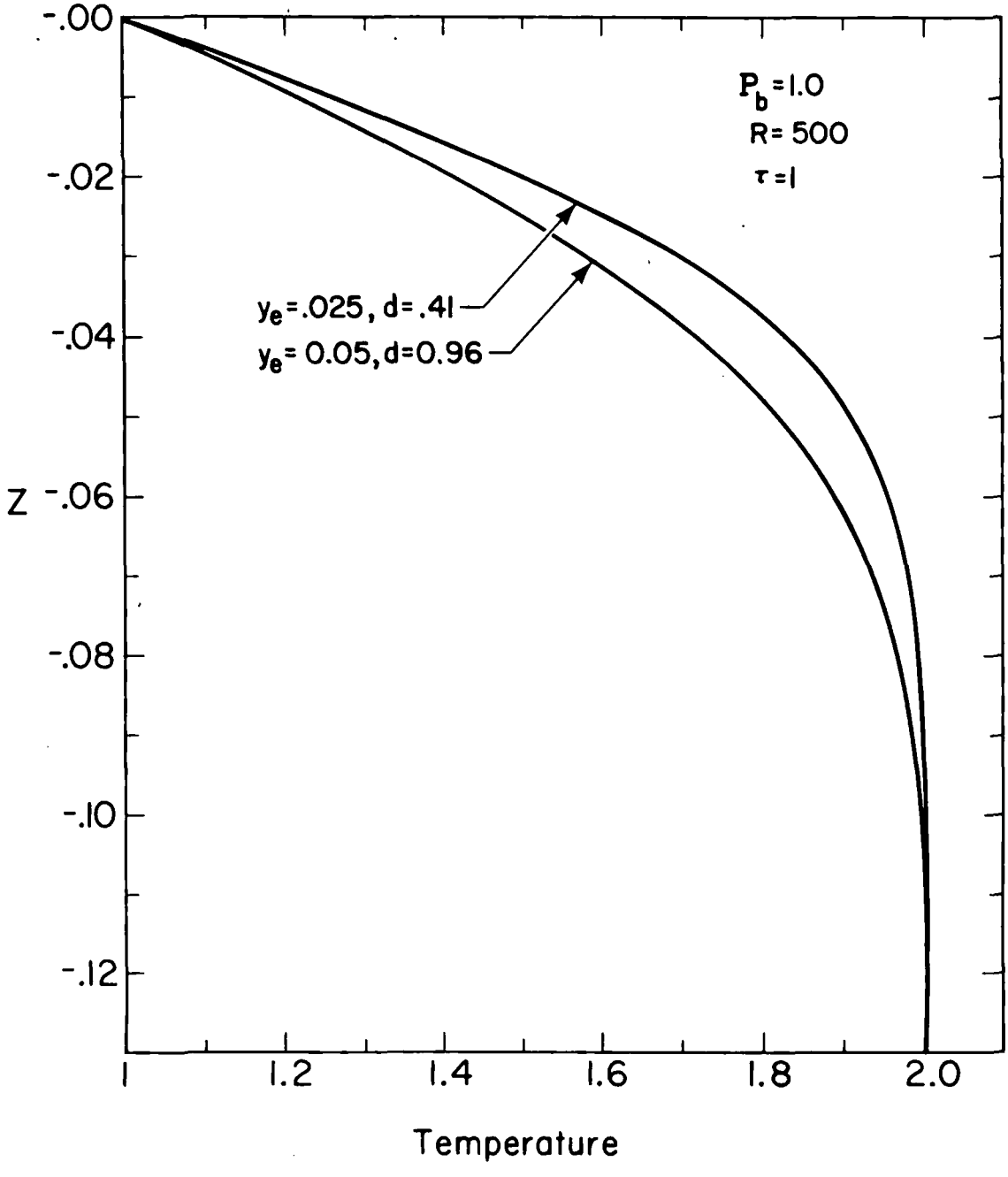

XBL 8012-13807

Fig. 11. Effect of semifault width on the boundary layer temperatures in the fault.

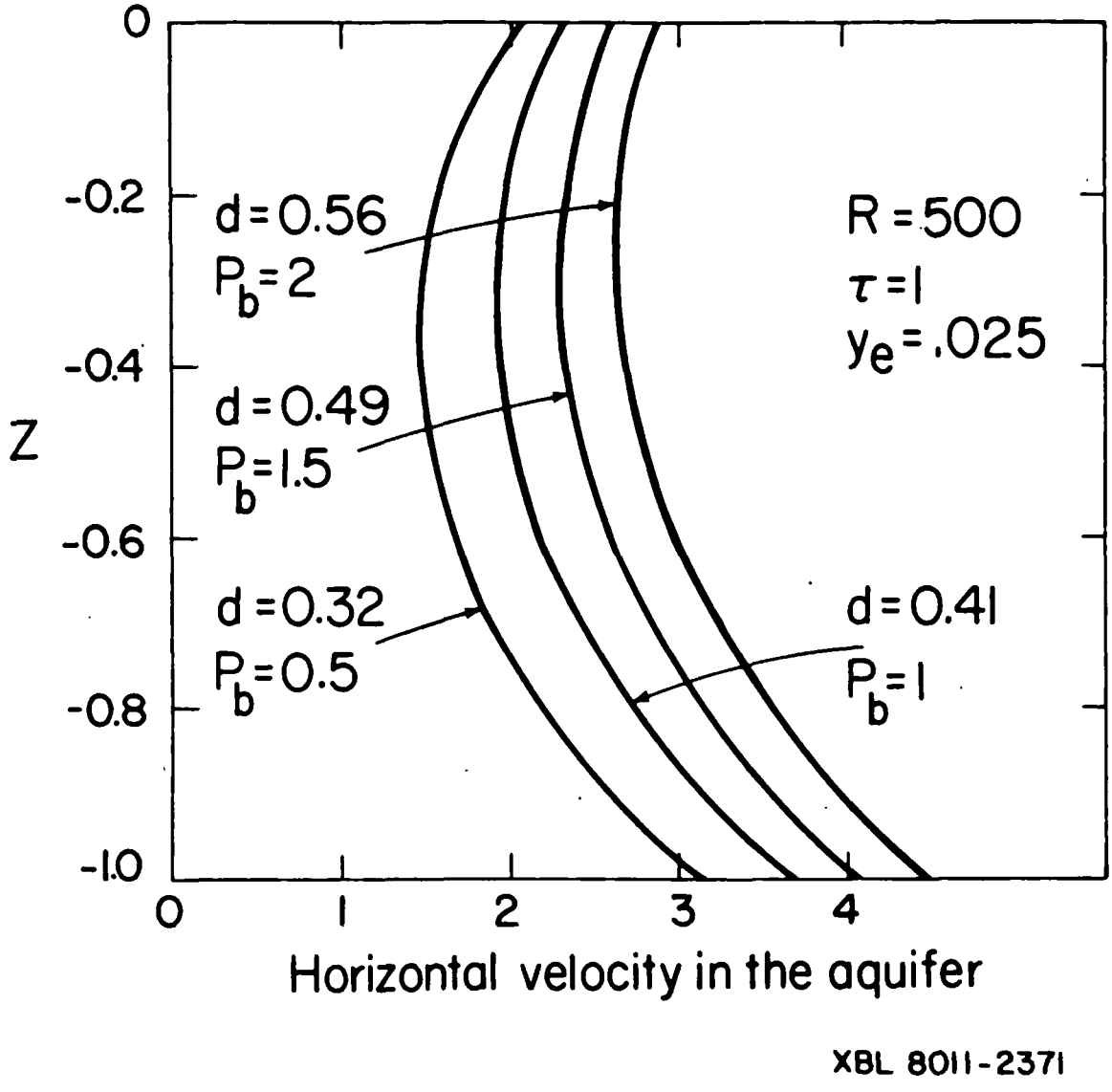

Fig. 12. Nondimensional horizontal liquid velocity in the aquifer along the depth of the reservoir for different values of P_b.

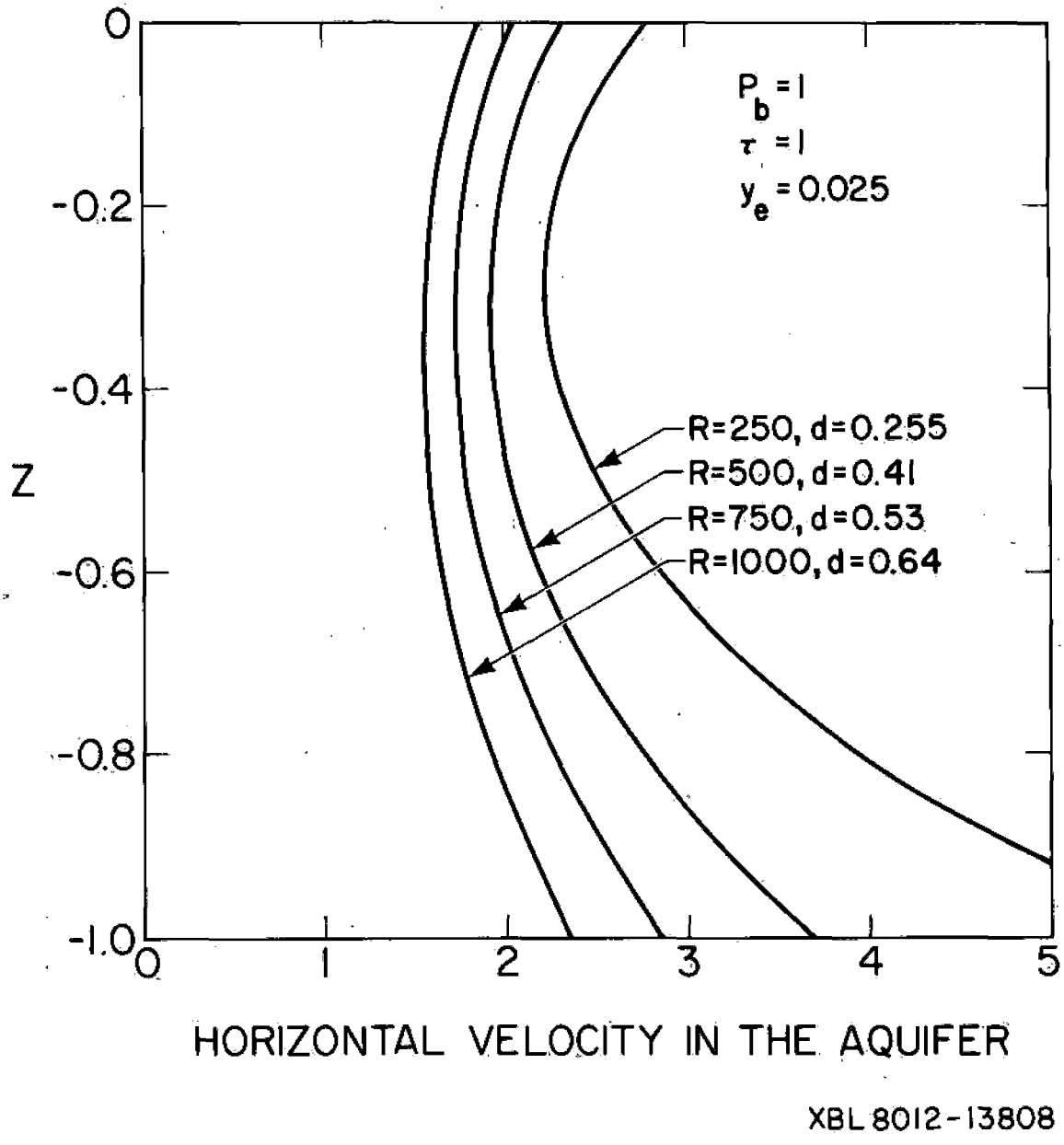

Fig. 13. Nondimensional horizontal velocity in the aquifer versus reservoir depth for various values of R.

nondimensional aquifer velocity $\bar{v}(\bar{z})$ is the ratio of $v'(z')$ and $y_e \rho_0' q_0'$. As discussed in Fig. 4, an increase in R is equivalent to an increase in the reference convection velocity q_0'. Therefore, the dimensional fluid velocity in the aquifer increases for higher R. It is consistent with the results of Fig. 4 where it is shown that the dimensional mass input to the system increases due to increased convection effects.

A plot of horizontal velocity in the aquifer versus depth is shown in Fig. 14 for different values of y_e. Note that the nondimensional velocities are lower for higher values of the fault width. However, as discussed in Fig. 5, the dimensional mass influx, into the reservoir is higher for larger values of y_e.

The fluid temperatures in the near fault regions of the aquifer are shown in Fig. 15 at different horizontal locations ($\bar{y} = y'/L'$) in the reservoir. Boundary layer temperatures in region 1, and in region 3 obtained from a quadrature solution (Eq. (39)) and a similarity solution (Eq. (41)) respectively are shown in this figure. As expected the quadrature solution matches the similarity solution for large values of $\bar{y}$ (y/y_e). The boundary layer temperatures decrease with increasing distance from the fault. This drop in temperatures is caused by heat loss to the surroundings through the cold upper boundary. The temperatures in the lower portions of the aquifer (regions 2 and 4) are constant and equal to the highest temperature value of $1 + \tau$. The fluid temperature in these regions remains at the supply temperature since heat loss is only confined to boundary layer

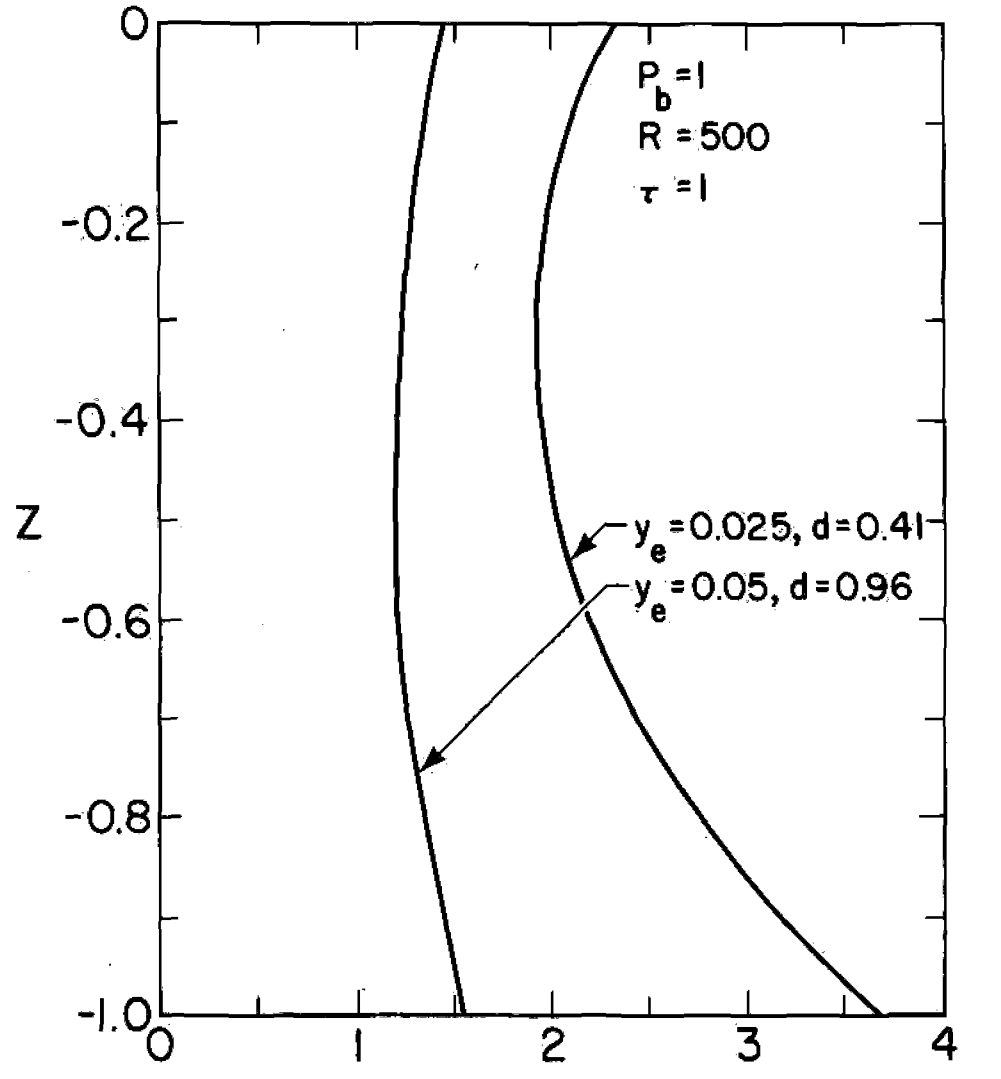

Fig. 14. Effect of semifault width on the nondimensional liquid velocity in the aquifer.

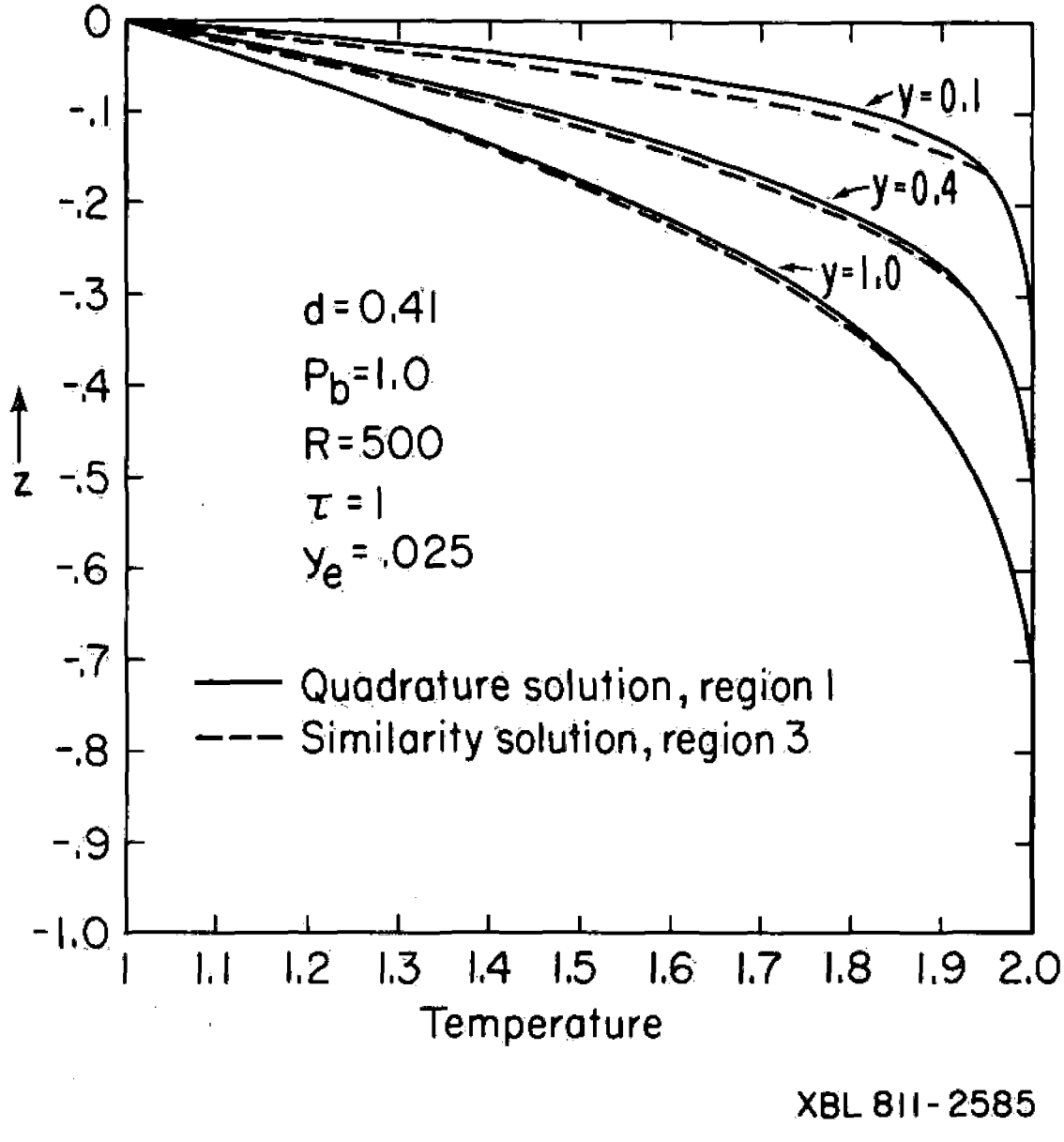

Fig. 15. Fluid temperatures in the near fault regions of the aquifer.

regions 1 and 3. Thus a hypothetical well drilled in regions 2 and 4 should encounter a zero vertical temperature gradient regime associated purely with a horizontal flow. In contrast, conventional wisdom suggests that the observation of small vertical temperature gradients implies vigorous vertical convection. Although it is true, on theoretical grounds, that the latter process will generate nearly isothermal regimes, it should be clear that specific geologic structure can have a similar influence.

Figure 16 shows the variations of the aquifer temperature with depth at several locations ($\hat{y} = y'/H'$) away from the fault. The $\hat{y} = 1$ represents the far end of the aquifer, which is located at d/y_e times its depth. The temperature decrease with increasing distance from the fault can be seen in the aquifer which is affected by heat loss through the cold upper boundary. At $\hat{y} = 0.1$, half of the aquifer is at least within 80 percent of the high temperature value.

Isotherms in the aquifer for the temperatures of Figs. 15 and 16 are shown in Fig. 17. Isotherms for $\hat{y} \to 0$ are obtained from the boundary layer temperatures Eqs. (39) and (41) and are shown by dashed lines. It may be noted that the horizontal temperature gradient decreases with increasing $\hat{y}$ and becomes vanishingly small for $\hat{y} \to 1$. $\theta_{\hat{y}}$-terms in Eq. (7b) becomes very small compared to vertical conduction terms θ_{zz}. Thus at this far field location, heat transfer is mainly controlled by vertical conduction.

Figure 18 shows the effect of fault inlet pressure on the surface temperature gradients both for the fault and the aquifer. Heat transfer at the surface increases with increasing P_b, as expected.

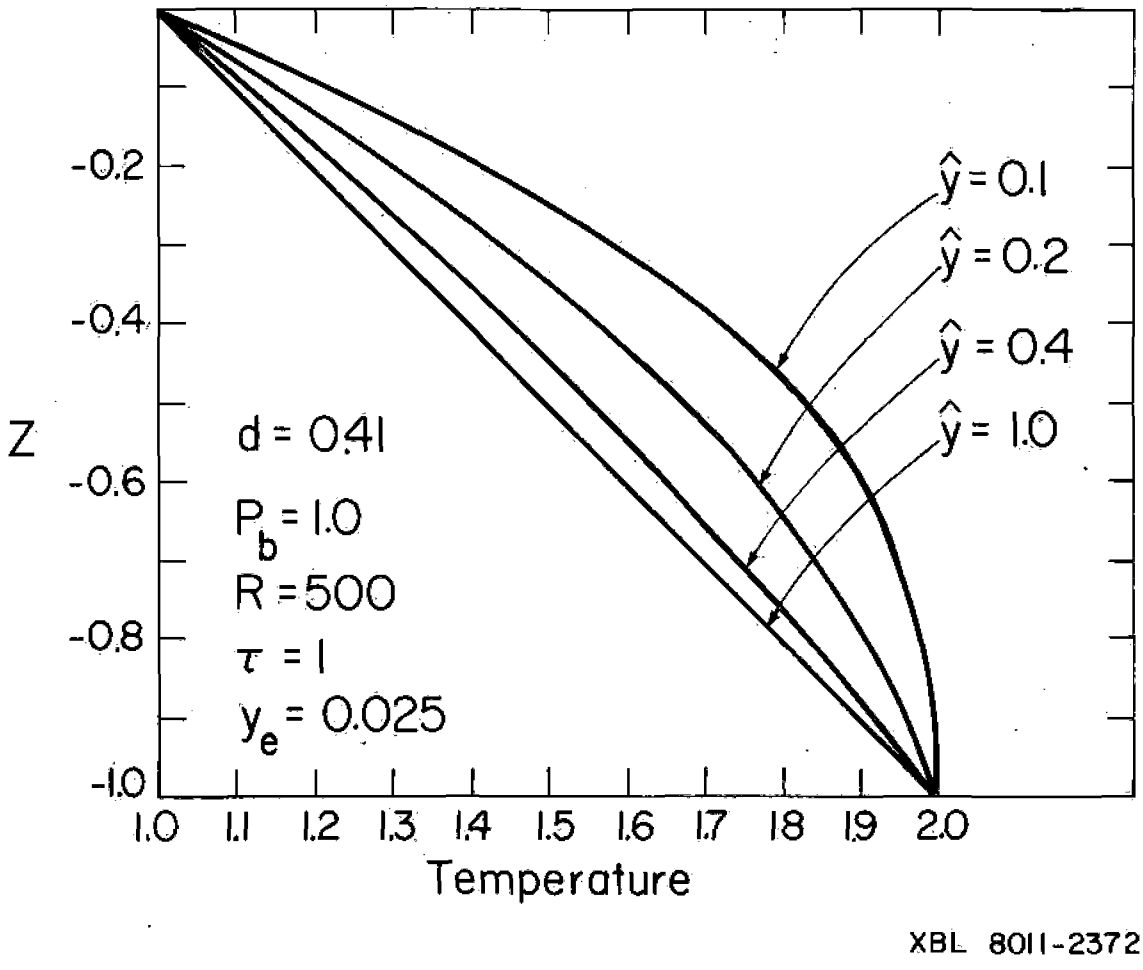

Fig. 16. Aquifer temperatures in the region 5.

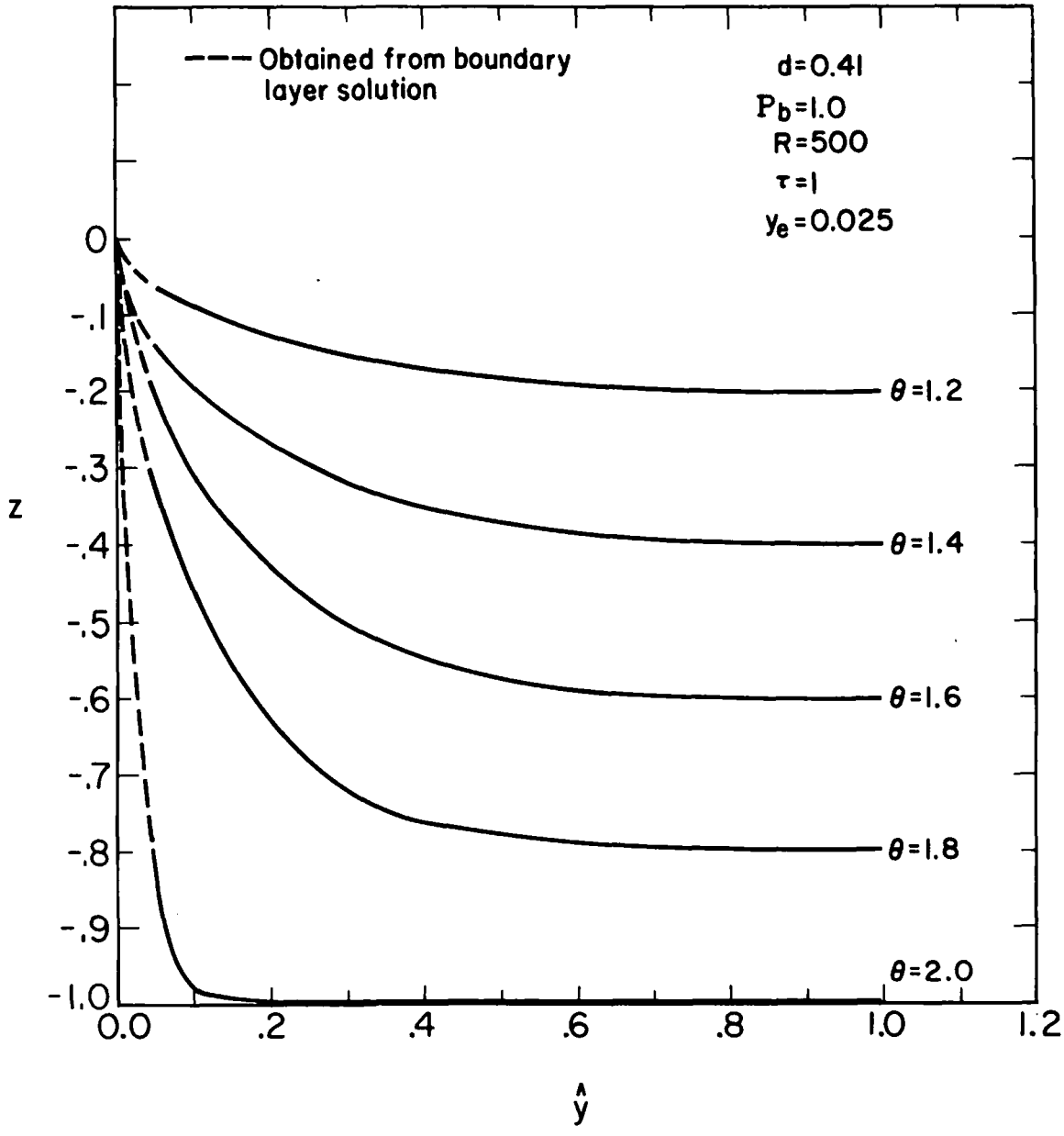

XBL 8012-13810

Fig. 17. Isotherms in the aquifer for the temperatures of the Figures 15 and 16.

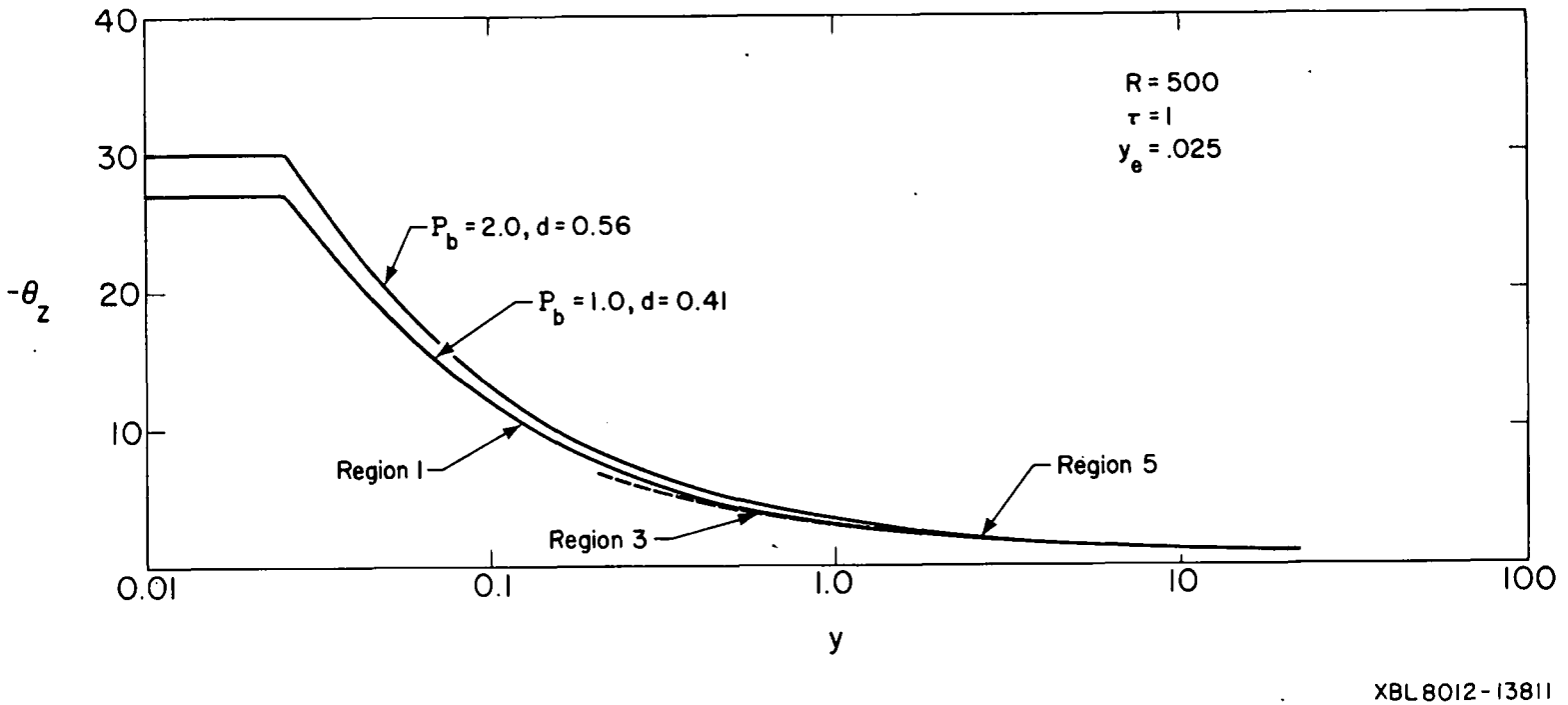

Fig. 18. Surface temperature gradients along the length of the aquifer for different values of P_b.

Matching of the three regions is shown for $P_b = 1$. It can be noted that the length of the aquifer is different for each P_b. This difference is due to different value of d associated with a different fault inlet pressure. The results imply that the fault zone convection heat transport enhances the surface heat flux by a factor of about 30 above the background conductive value.

This value is the right order of magnitude for geothermal systems with vigorous surface manifestations where heated water is present in an extensive region just below the surface. It is rather large for systems exemplified by East Mesa, Imperial Valley, California where the reservoir is separated from the surface by an extensive region of clay rich sediments. For East Mesa, the heat flux near the fracture zone is about three to four times the background value (Goyal and Kassoy [17]).

Effect of the Rayleigh number on the surface heat flux is shown in Fig. 19. Temperature gradients at the surface increase for higher values of R. Increased convection effects associated with larger values of R are expected to enhance the surface heat flux as shown in Fig. 19.

Surface temperature gradients for different fault widths (y_e) are shown in Fig. 20. Two different values of y_e are used in this figure. Temperature gradients up to $y = 0.025$ and 0.05 are constant and represent the fault zone where these do not change with respect to y and are only function of depth as discussed in the section of fault zone solutions. However, gradients do decrease with y in the aquifer as shown in Fig. 20. It may be noted that the surface heat flux for

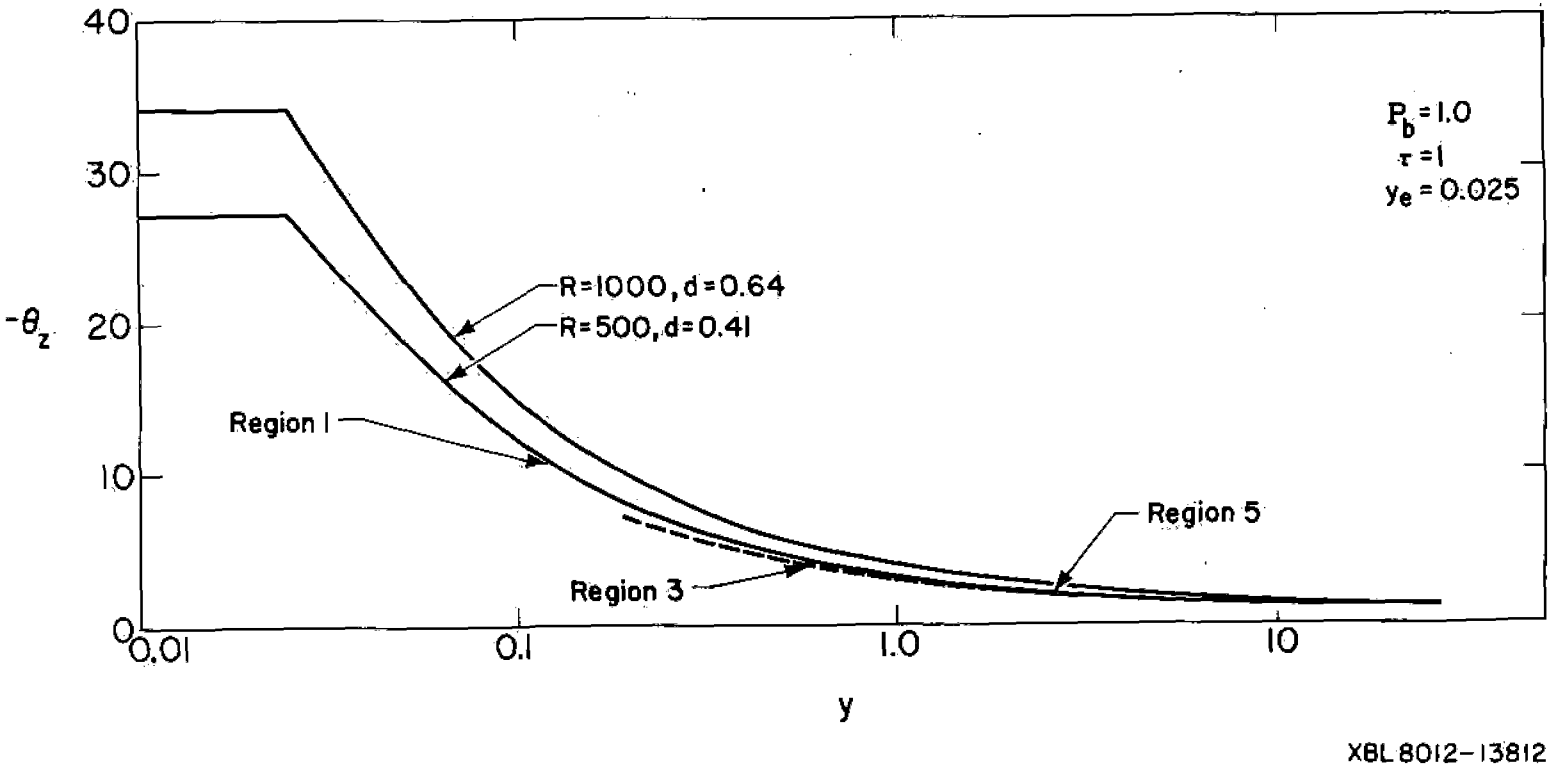

Fig. 19. Surface heat flux versus aquifer length for different values of Rayleigh number.

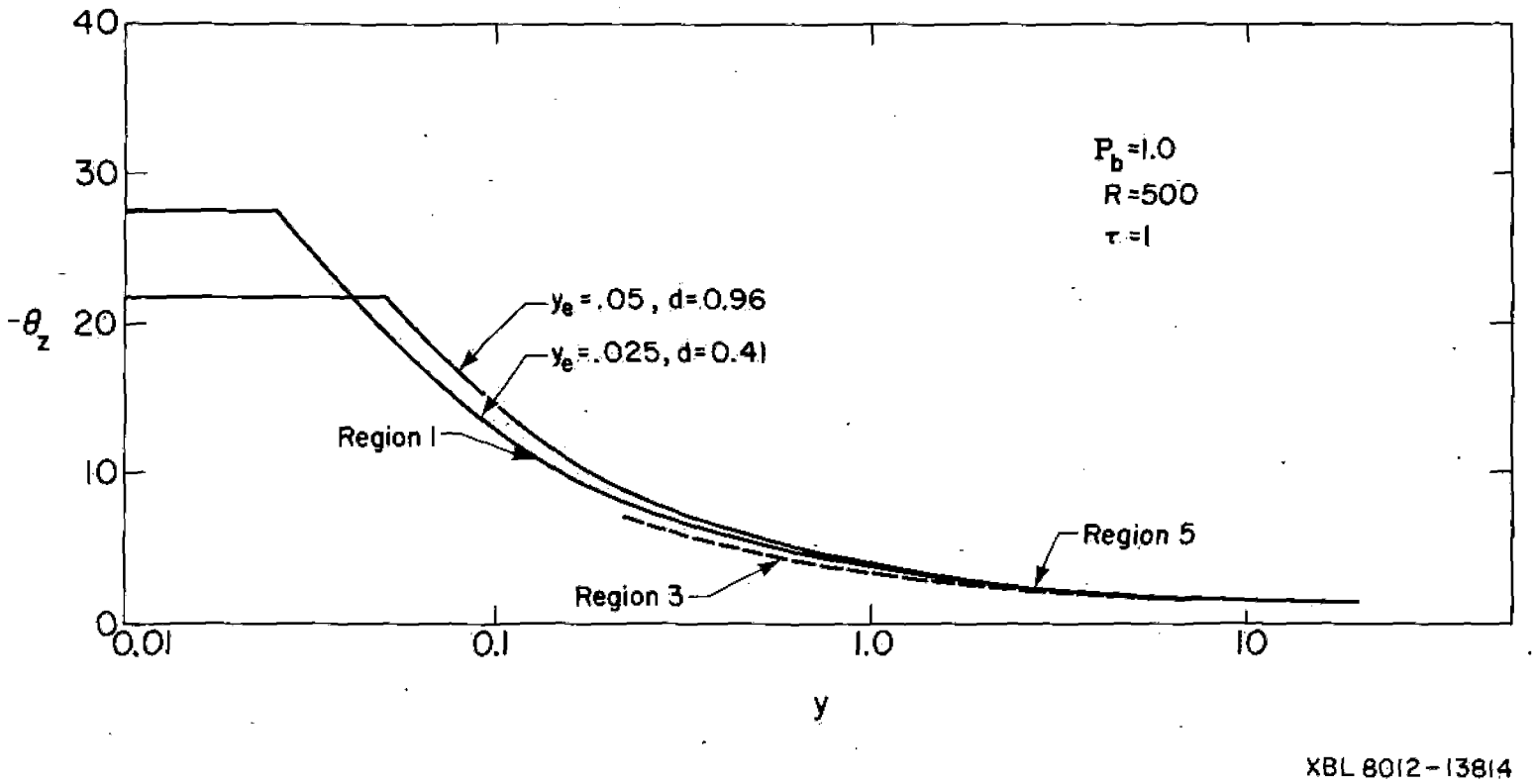

Fig. 20. Effect of fault width on the surface heat transfer.

y_e = 0.05 is lower in the fault zone and higher in the aquifer compared to that for y_e = 0.025. Lower temperature gradients in the fault zone for y_e = 0.05 are due to reduced convection effects as discussed in Figs. 5 and 11. Higher heat flux in the aquifer for y_e = 0.05 is associated with increased mass flux through the fault-aquifer system as also discussed in Fig. 5.

The effect of the overheat ratio (τ) on the surface heat flux is shown in Fig. 21. As expected, heat transfer increases with increasing value of τ. Surface heat flux for τ = 2 is twice that obtained for τ = 1 throughout the fault aquifer system; including the far field boundary. This is consistent with eqs. (1) and (10b) where an increase in τ enhances the hot bottom boundary temperature (T'_{max}) and the specified temperature at the far field boundary respectively.

Figure 22 shows the effect of prescribed boundary conditions M and P_b on the length of the aquifer d. M, the nondimensional mass input to the fault, is the ratio of M' and reference mass flow rate M'_o ($=2\, y'_e \rho'_o q'_o$) as defined in Goyal and Kassoy [9]. An increase in M increases d significantly more than a corresponding increase in P_b. It may be noted in this figure that a change in P_b from 1 to 2 is equivalent to an increase in M from 2.65 to 3.55 i.e. a 100 percent increase in the prescribed inlet pressure results only in a 30 percent increase in the input mass to the system. It suggests that the enlargement of the isothermal region in the aquifer is stronger when the input mass is doubled compared to that when inlet pressure is doubled.

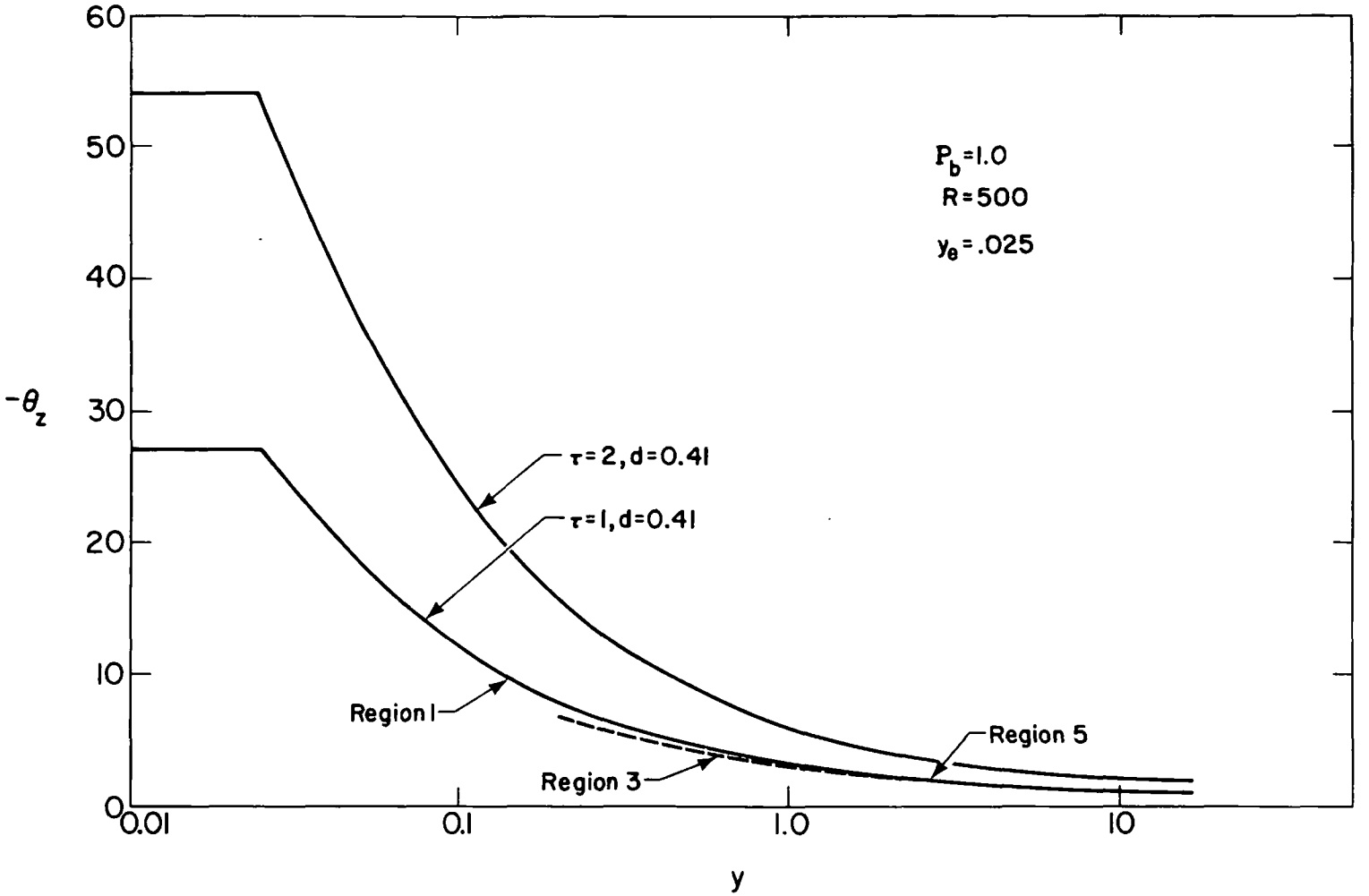

Fig. 21. Effect of overheat ratio (τ) on the surface heat flux in the fault-aquifer system.

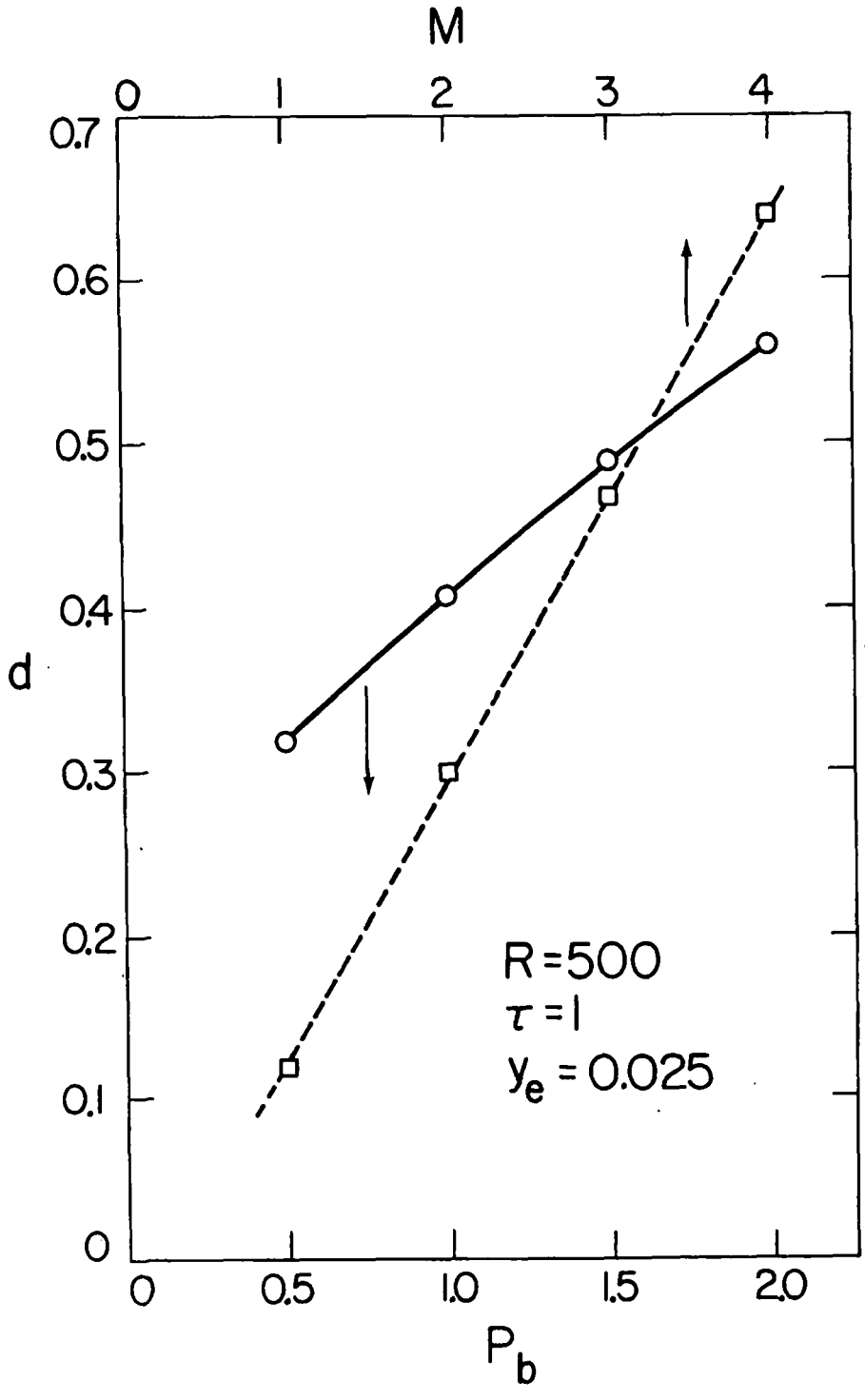

XBL 8011-2367

Fig. 22. A comparison between the plots of M versus d and P_b versus d. (The data of M versus d from Goyal and Kassoy [9]).

A FIELD EXAMPLE

We shall now qualitatively validate the model profiles (Figs. 15 and 16) with a field example from East Mesa, California.

The geothermal reservoir in East Mesa lies at a depth of about 800 meters from the ground surface (Goyal and Kassoy [17]). The downhole temperatures measured in various wells tapping the permeable zones are shown in Fig. 23. The temperatures measured in the conduction dominated upper 800 meters are not shown in this figure, while Figures 15 and 16 show the ambient temperature at the upper boundary of the reservoir as prescribed. For a proper comparison, it is desirable to include a clay cap in the model being studied. In that case, large temperature gradients at the upper boundary of the reservoir ($z = 0$) caused by prescribed ambient temperature boundary condition will disappear as discussed in Goyal and Kassoy [17]. However, the heat transfer mechanism in the model being studied and that shown in Figure 23 is similar if we replace the upper boundary of our model by an interface between the reservoir and the clay cap where the temperature will be much higher than the ambient temperature and will decrease with the distance away from the fault due to heat loss to the surface through the clay cap. Thus a qualitative comparison is possible between Figures 15, 16 and 23. It can be seen that wells 6-1, 6-2, 8-1, 44-7 and 48-7 are located in the hottest portions of the reservoir. A qualitative comparison of the borehole temperature variations in Fig. 23 and theoretical predictions in Figs. 15 and 16 shows that the temperature profiles in wells 6-1, 6-2, 8-1, 44-7 and 48-7 are

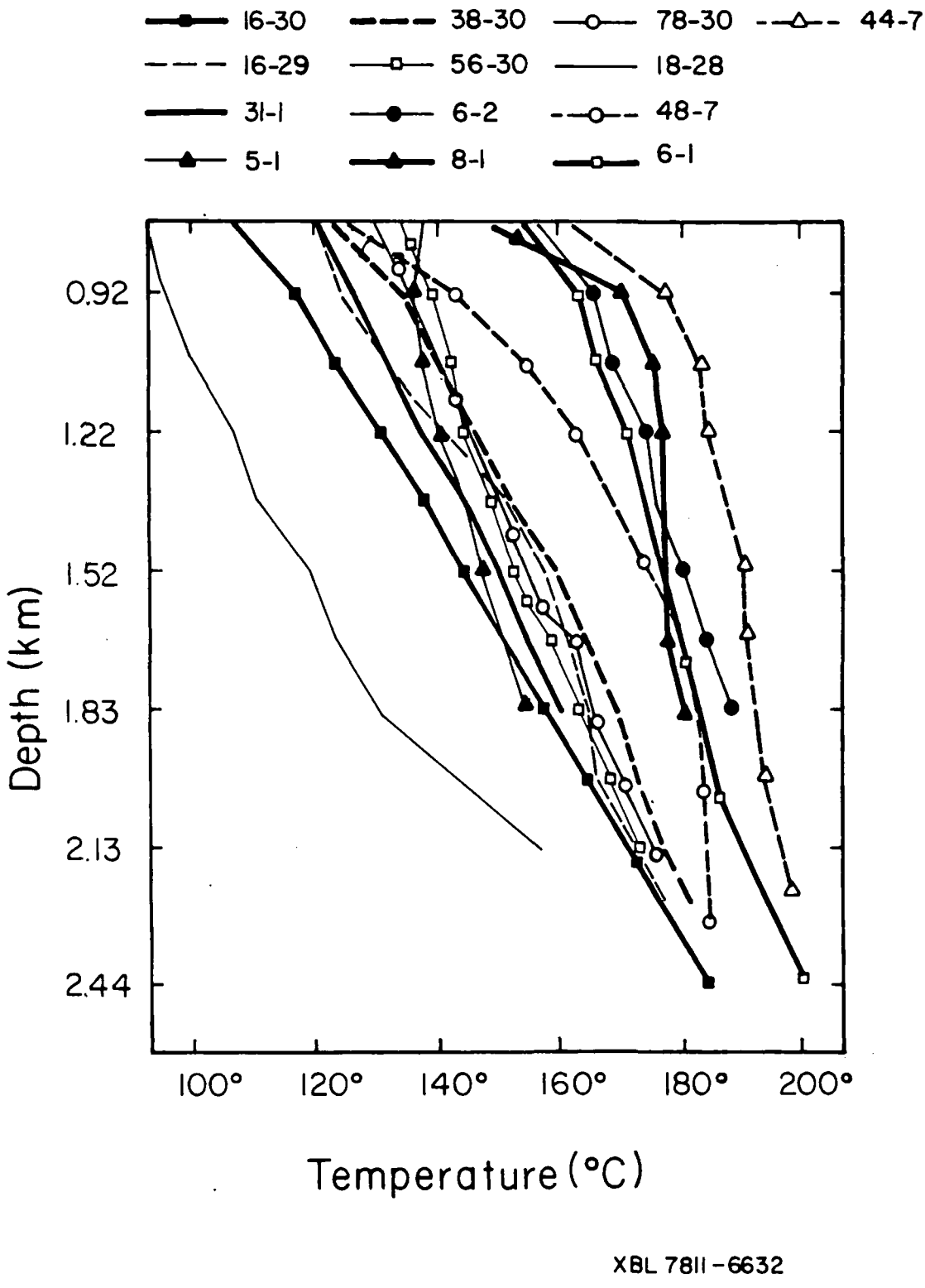

Fig. 23. Temperature-depth profile for East Mesa Wells below 800 meters depth (from Goyal and Kassoy [17]).

similar to those in Fig. 15 pertaining to the near fault regions. This suggests that the aforementioned wells are at least close to the hot recharge zones of this field. In fact, constant temperature profiles similar to those in Fig. 15 can be seen in wells 8-1, 44-7 and 48-7 between depths of 1200-1800 meters, 1500-1850 meters and 1800-2100 meters respectively. The temperature profiles of the other wells in Fig. 23 are similar to those in Fig. 16 for $y > 0.4$. These wells are thought to be farther away from the intensely fractured zone of the reservoir system. In particular, well 18-28 is farthest from any known fault zone. Comparison of Figs. 15, 16 and 23 shows that the model predictions are credible at least in a qualitative sense.

APPLICATION TO A TYPICAL GEOTHERMAL SYSTEM

This theory can be used to predict the velocities, pressures, temperatures, and heat flux at different locations in the fault and the aquifer in undeveloped systems. Let us consider a geothermal system with the following typical data:

$y_e' = 75$ m

$L' = 3000$ m

$T_o' = 298$ K

$\Delta T' = 90$ K

$K' = 2 \times 10^{-13}$ m^2

$P_b' = 300 \times 10^5$ Pascals

$\lambda_m' = 5.1 \times 10^{-3}$ cal/cm-sec-K (Goyal and Kassoy [17])

using the physical properties of the water at 25°C, the following reference values can be calculated:

$q_o' = 4.44$ mm/day

$p_o' = 6.87 \times 10^5$ Pascals.

The corresponding nondimensional numbers are:

$y_e = 0.025$

$R \simeq 300$

$P_b \simeq 1$

$\tau \simeq 0.3$

The corresponding values of d and H' for this set of non-dimensional numbers are 0.29 and 34.8 km respectively.

A plots of the horizontal velocity (mm/day) in the aquifer and the overpressure (Pascals) associated with fluid motion at fault-aquifer interface at various depths are shown in Figs. 24 and 25 respectively.

The heat flux (HFU) at the surface is shown in Fig. 26. The background heat flow of about 1.5 HFU is the world-wide average heat flux for a normal temperature gradient of 30°C/km as assumed in this case.

CONCLUSIONS

Quasi-analytic solutions are obtained for velocities, pressures, temperatures and temperature gradients in a fault-controlled liquid dominated geothermal system with a specified pressure at the fault inlet. The solution techniques involve the combination of perturbation methods, boundary layer theory and numerical methods. The effect of various parameters such as fault inlet pressure, Rayleigh number, overheat ratio and fault width are investigated on these solutions.

The analysis can be applied to compute the velocity field in an aquifer in response to changes in its permeability or fluid viscosity under a prescribed inlet pressure. Also, if the geological, geophysical, heat flux and borehole logging data is known, it is possible to calculate total fluid recharge rate to the geothermal system in addition to other physical parameters of interest.

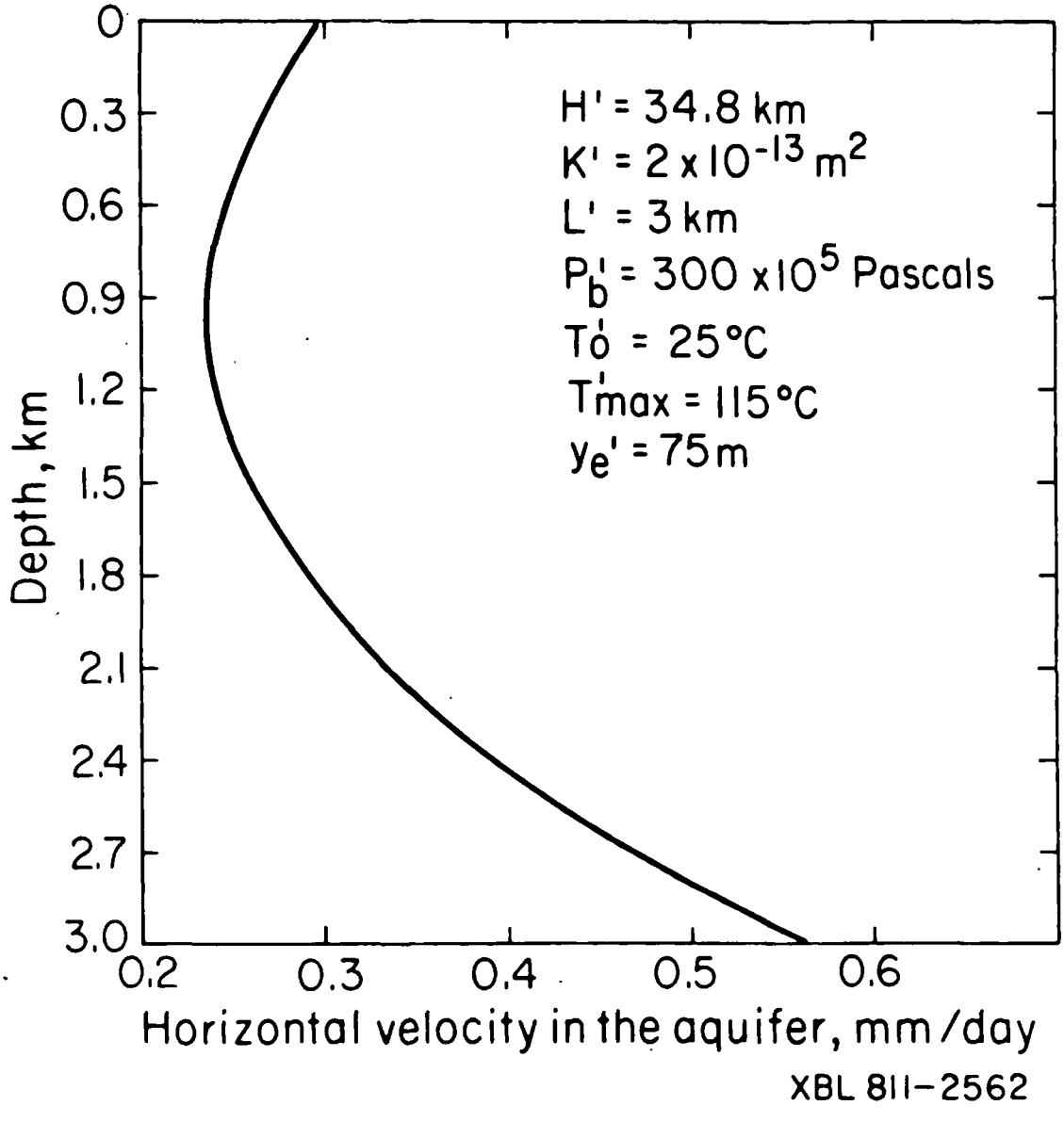

Fig. 24. Liquid velocity in the aquifer versus reservoir depth.

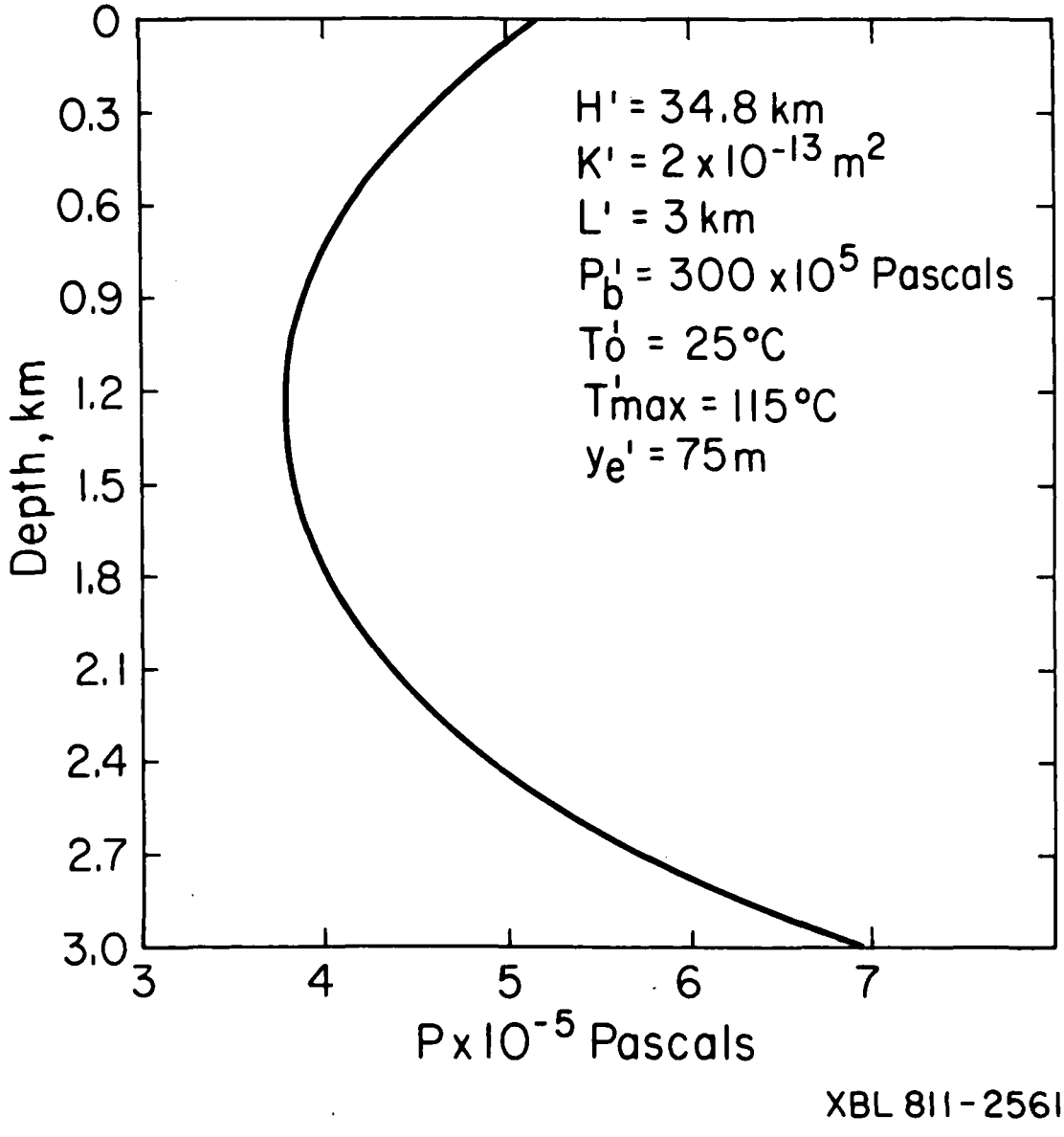

Fig. 25. Overpressures at the fault aquifer interface versus reservoir depth.

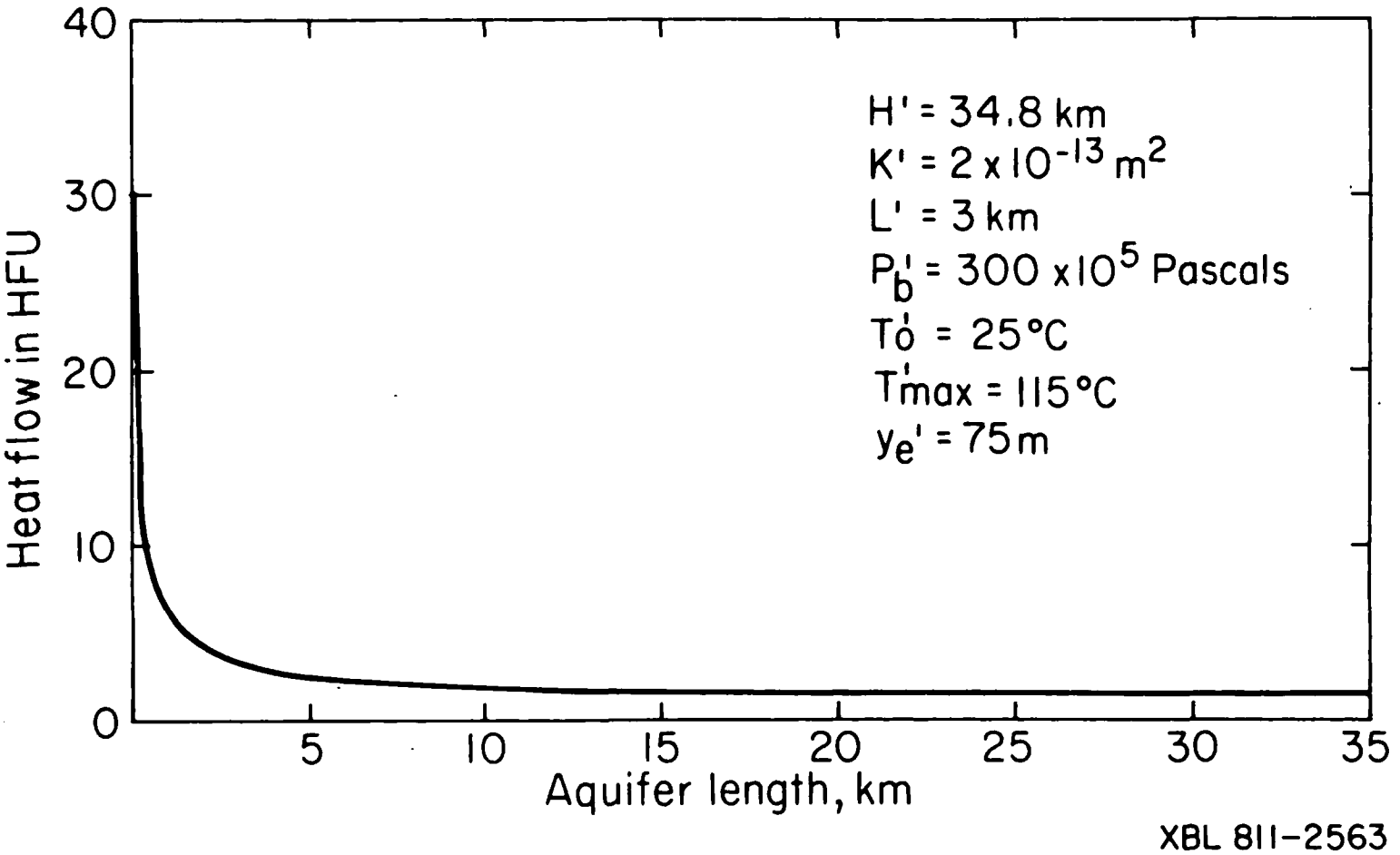

Fig. 26. Surface heat flow along the length of the aquifer.

It is shown that very small vertical temperature gradients in the near fault regions 2 and 4 can be associated with purely horizontal water motion (Darcy flow rate of about 0.02 cm/day near the hypothesized fault) rather than only with the more vigorous upflow itself. While it is clear on theoretical grounds that the latter process will generate nearly isothermal regimes, it should be clear that specific geologic structure can have a similar effect. Thus it is reasonable to speculate that deep, high temperature, isothermal zones are at least near to the source of a geothermal system.

The concepts used to generate the model can be tested directly by comparison of the field data and the theoretical prediction. Current measurement techniques provide surface heat flux distributions, downhole temperature and pressure distributions which can be compared with values obtained in a given model. The temperatures predicted by this model compare favorably in a qualitative sense to those measured in the East Mesa anomaly.

ACKNOWLEDGMENT

The authors would like to thank David Kassoy of the University of Colorado, Boulder, Jack Howard, Sally Benson and Karsten Pruess of LBL for very constructive criticism.

This work was supported by the Assistant Secretary for Conservation and Renewable Energy, Office of Renewable Technology, Division of Geothermal and Hydropower Technologies, of the U. S. Department of Energy under Contract No. DE-AC03-76SF00098.

APPENDIX

The dimensional equations describing the conservation of mass, momentum and energy in a fault-aquifer system, as obtained from Goyal [16] can be written as

Fault zone:

$$V'_{y'} + W'_{z'} = 0 \tag{A1}$$

$$V' = -\frac{K'}{\nu'} P'_{y'} \quad , \quad W' = \frac{K'}{\nu'} \left\{ -(P' - p'_H)_{z'} + g' \rho'_o \alpha'_e (T' - T'_o) \right\} \tag{A2a,b}$$

$$C'_p \left[V'T'_{y'} + W'T'_{z'} \right] = \lambda'_m \left\{ T'_{y'y'} + T'_{z'z'} \right\} \tag{A3}$$

Aquifer:

$$v'(z') = -\frac{K'}{\nu'} p'_{y'} \tag{A4}$$

$$C'_p v' \theta'_{y'} = \lambda'_m (\theta'_{y'y'} + \theta'_{z'z'}) \tag{A5}$$

The solution of the above system is subject to the following boundary and continuity conditions.

Boundary conditions:

Fault zone:

$$W'(y',0) = 0 \quad , \quad P'(y',-L') = P'_b \tag{A6a,b}$$

$$T'(y',0) = T'_o \quad , \quad T'(y',-L') = T'_{max} \quad , \quad T'_{y'}(0,z') = 0 \tag{A7a-c}$$

These conditions describe an impermeable upper boundary, fault pressure at the bottom of the reservoir, the cold upper boundary, the hot lower boundary and system symmetry respectively.

Aquifer:

$$\theta'(y',0) = T_o' \quad , \quad \theta'(y',-L') = T_{max}' \quad , \tag{A8a,b}$$

$$\theta'(H',z') = T_o' - (T_{max}' - T_o') \frac{z'}{L'} \tag{A9}$$

The aquifer equations describe the temperatures at the cold upper boundary, the hot lower boundary and at the far field boundary of the aquifer. Equation (A9) is a formal statement of the required conduction-controlled heat transfer at the aquifer edge.

Continuity conditions at the fault-aquifer boundary:

$$T'(y_e',z') = \theta'(y_e',z') \quad , \quad V'(\pm y_e',z') = \pm v'(z') \tag{A10a,b}$$

$$P'(y_e',z') = p'(y_e',z') \tag{A11}$$

These equations describe the continuity of temperature, velocity and pressure respectively.

The system of Eqs. (A1) to (A11) is first non dimensionalized and then solved as discussed in the text of the paper.

REFERENCES

1. Combarnous, M. A. and S. A. Bories. Hydrothermal Convection in Porous Media. Advances in Hydrosciences, 10, 232-307, 1975.
2. Cheng, P., "Heat Transfer in Geothermal Systems," in Advances in Heat Transfer, 14 (ed. T. F. Irvine, Jr. and J. P. Hartnett), Academic press, NY, 1-105, 1978.
3. Garg, S. K. and D. R. Kassoy. Convective Heat and Mass Transfer in Hydrothermal Systems, Geothermal Resources (eds. L. Ryback and P. Muffler), Johy Wiley and Sons, Ltd., London, 1979.
4. Einarsson, T., The Nature of the Springs of iceland (in German), Rit, Visind. Esl. 26, 1, 1942.
5. Wooding, R. A., Steady State Free Thermal Convection of Liquid in a Saturated Permeable Medium, J. Fluid Mechanics, 2, 273-285, 1957.
6. Elder, J. W., Heat and Mass Transfer in the Earth's Hydrothermal Systems, New Zealand D. S. I. R. Bulletin 169, 1966.
7. Donaldson, I. G., A Possible Model for Hydrothermal Systems and Methods of Studying Such a Model. Third Australian Conference on Hydraulics and Fluid Mechanics, Inst. of Eng. Aust. and Univ. of N. S. W., Sidney, 202-204, 1968.
8. Donaldson, I. G., The Simulation of Geothermal Systems with a Simple Convection Model. Geothermics, special issue 2, 649-654, 1970.
9. Goyal, K. P. and D. R. Kassoy, "Fault Zone Controlled Charging of a Liquid-Dominated Geothermal Reservoir," J. Geophysical Res., vol. 85, No. B4, 1867-1875, April 1980.

10. Mercer, J. W., C. F. Pinder, and I. G. Donaldson. A Galerkin-Finite Element Analysis of the Hydrothermal System at Wairakei, New Zealand. J. of Geophysical Research, 80(17), 2608-2621, 1975.

11. Mercer, J. W. and C. R. Faust, Geothermal Reservoir Simulation III: Application of Liquid and Vapor-Dominated Hydrothermal Techniques to Wairakei, New Zealand, Water Resources Research, 15(3), 653-671, 1979.

12. Sorey, M. L., A Model of the Hydrothermal System of Long Valley Caldera, California, Summaries, Second Workshop Geothermal Reservoir Engineering, Stanford, California, 324-338, 1976.

13. Riney, T. D., J. W. Pritchett, and S. K. Garg, Salton Sea Geothermal Reservoir Simulations, Proceedings, Third Workshop Geothermal Reservoir Engineering, Stanford University, Stanford, California, 178-184, 1977.

14. Lippmann, M. J. and K. P. Goyal, Numerical Modelling Studies of the Cerro Prieto Reservoir, Lawrence Berkeley Laboratory, University of California, Berkeley, LBL-9590, Cerro Prieto-14, 11, February 1980.

15. Pritchett, J. W., L. F. Rice and S. K. Garg, Reservoir Simulation Studies: Wairakei Geothermal field, New Zealand, Lawrence Berkeley Laboratory, University of California, Berkeley, LBL-11497, GREMP-11, UC-66, p. 103, 1980.

16. Goyal, K. P., Heat and Mass Transfer in a Saturated Porous Medium with Applications to Geothermal Reservoirs, Ph. D. Thesis, Mechanical Engineering Department, University of Colorado, Boulder, 294, 1978.

17. Goyal, K. P. and D. R. Kassoy, "A Plausible Two Dimensional Vertical Model of the East Mesa Geothermal Field, California U. S. A," J. of Geophys. Res., Vol. 86, B11, pp. 10719-10733, 1981.

18. Grindley, G. W., The Geology, Structure and Exploitation of the Wairakei Geothermal Field, Taupo, New Zealand, 131, 1965.

19. Grindley, G. W., Subsurface Structures and Relation to Steam Production in the Broadlands Geothermal Field, New Zealand, Geothermics: Proceedings of the United Nations Symposium on the Development and Utilization of Geothermal Resources, Vol. 2, part 1, special issue, 248-261, 1970.

20. Rinehart, C. D., and D. C. Ross, Geology and Mineral Deposits of the Mount Morrison Quadrangle, Sierra Nevada, California, U. S. Geological Survey, Professional Paper No. 385, 106, 1964.

21. Elders, W. A., R. W. Rex, T. Meidav, P. T. Robinson, and S. Biehler. Crustal Spreading in Southern California, Science, 178, 15-24, 1972.

22. Puente, C. I., and A. de la Pena, L., "Geology of the Cerro Prieto Geothermal field," in the Proceedings of the First Symposium on the Cerro Prieto Geothermal Field, Baja California, Mexico, Lawrence Berkeley laboratory, University of California, Berkeley, LBL-7098, 17-40, 1978.

23. Ward, P. L. and K. H. Jacobs, Microearthquakes in the Ahuachapan Geothermal Field, El Salvador, Central America, Science, 173, 328-330, 1971.

24. Combs, J. and D. Hadley, Microearthquake Investigation of the Mesa Geothermal Anomaly, Imperial Valley, California, Geophysics, 42(1), 17-33, 1977.

25. Bailey, T. P., A Hydrogeological and Subsurface Study of Imperial Valley Geothermal Anomalies, Imperial Valley, California, Geological Science, University of Colorado unpublished report, 101, 1977.

26. Eckhaus, V., Matched Asymptotic Expansions and Singular Perturbations, Elsevier Publishing Co., Inc., New York, 1973.

27. Benson, S. M., G. S. Bodvarsson and D. C. Mangold, Reservoir Engineering of Shallow, Fault Charged Hydrothermal Systems, LBL-13271, Lawrence Berkeley Laboratory, University of California, Berkeley, December 1981.

Table 1.

d	P_b	R	τ	y_e
0.32	0.5	500	1	0.025
0.41	1	500	1	0.025
0.49	1.5	500	1	0.025
0.56	2	500	1	0.025
0.255	1	250	1	0.025
0.53	1	750	1	0.025
0.64	1	1000	1	0.025
0.96	1	500	1	0.05
0.41	1	500	2	0.025

FIGURE CAPTIONS

Fig. 1. Two-dimensional conceptual model of a liquid dominated geothermal reservoir.

Fig. 2. Five different regions in the aquifer.

Fig. 3. Vertical velocity distributions along the depth of the fault for various values of P_b.

Fig. 4. Effect of Rayleigh number on the vertical velocity in the fault.

Fig. 5. Vertical velocity in the fault versus depth for different fault widths.

Fig. 6. Fault overpressures versus depth for various values of P_b.

Fig. 7. Effect of Rayleigh number on the fault overpressure.

Fig. 8. Fault overpressures versus depth for different values of y_e.

Fig. 9. Fluid temperatures in the fault for various values of P_b.

Fig. 10. Fluid temperatures in the fault versus depth for various values of R.

Fig. 11. Effect of semifault width on the boundary layer temperatures in the fault.

Fig. 12. Nondimensional horizontal liquid velocity in the aquifer along the depth of the reservoir for different values of P_b.

Fig. 13. Nondimensional horizontal velocity in the aquifer versus reservoir depth for various values of R.

Fig. 14. Effect of semifault width on the nondimensional liquid velocity in the aquifer.

Fig. 15. Fluid temperatures in the near fault regions of the aquifer.

TECHNICAL INFORMATION DEPARTMENT
LAWRENCE BERKELEY LABORATORY
UNIVERSITY OF CALIFORNIA
BERKELEY, CALIFORNIA 94720